X-Ray Imaging for Environmental Applications

Franco Zanini

Elettra - Sincrotrone Trieste

The Italian synchrotron light laboratory - Elettra

The SYRMEP beamline @ Elettra

Designed and constructed in collaboration with *INFN* and the *Physics Dept. of Università di Trieste*. Dedicated to **absorption** and **phase-sensitive** hard **X-ray imaging techniques.**

Medical applications

- *ex-vivo* experiments

- *in-vivo* studies → mammography
  → small animals

Material science and cultural heritage studies

- study of microstructural properties → in a very large range of materials

- *in-situ* and real-time experiments → growth processes
  → mechanical and thermal treatments
  → phase transitions ….

The SYRMEP beamline layout

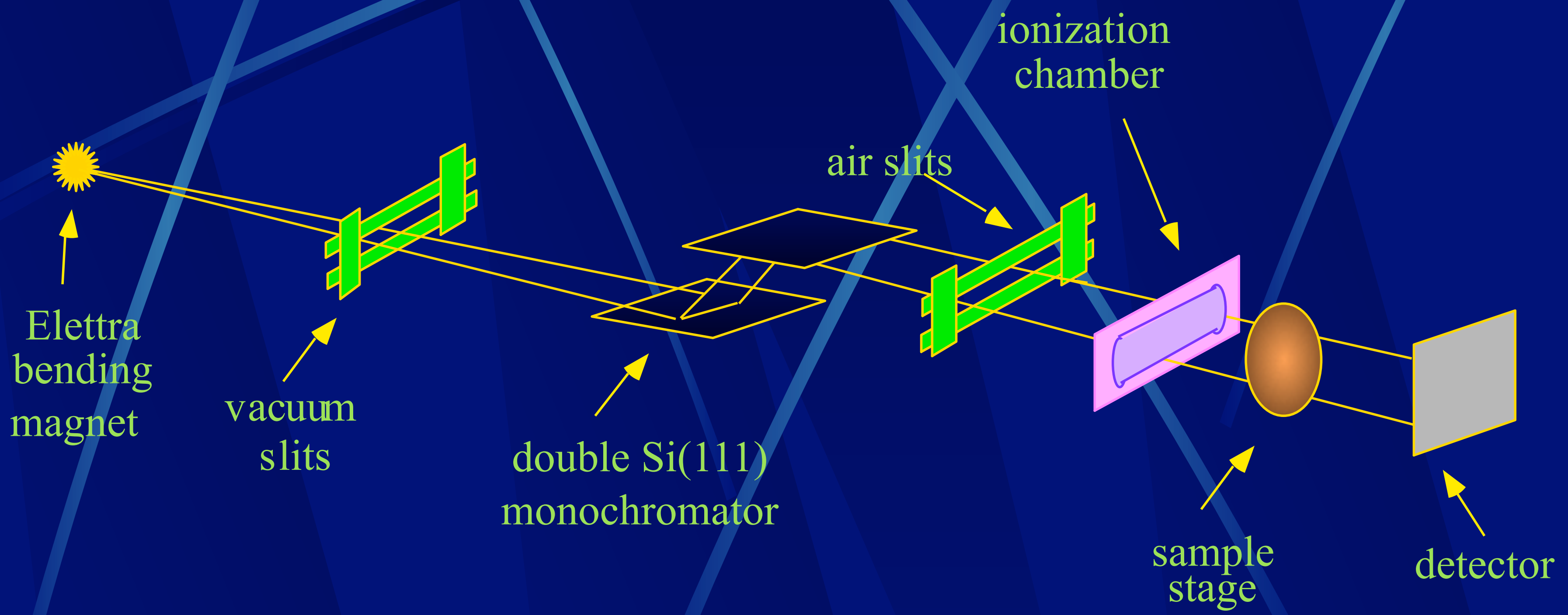

- Energy range: **8.3 ÷ 35 keV**, Bandwidth **$\Delta E/E \cong 2\times10^{-3}$**
- Beam size at sample (h x v) ≅ **150 mm x 4-6 mm**
- Source size (FWHM) s (h x v) ≅ **230 µm x 80 µm**
- Typical fluxes @15 keV ≅ $7 * 10^8$ phot./mm^2 s (@ 2.4 GeV, 180 mA)
- Source-to-sample distance: **D ≅ 23 m**

Why X-ray imaging at a 3rd generation SR facility?

- high energy photons and high flux
  - → **heavy** and/or **bulky samples** in transmission geometry
  - → **tunability** in a large energy range (dose reduction)
  - → **short** exposure times

- small angular source size and big source-to-sample distance
  - → **high spatial resolution** ($\rho = s\, d / D$ <≈ 1 μm at SYRMEP)
  - → possibility of **big sample-to-detector distances** (d<≈ 1m at SYRMEP)
  - → **high** spatial **coherence** of the X beam ($L_c = \lambda\, D/(2\, s) \cong 10\mu m$ @15keV)

→ ***Phase-sensitive techniques***

Absorption and Phase-Contrast radiography

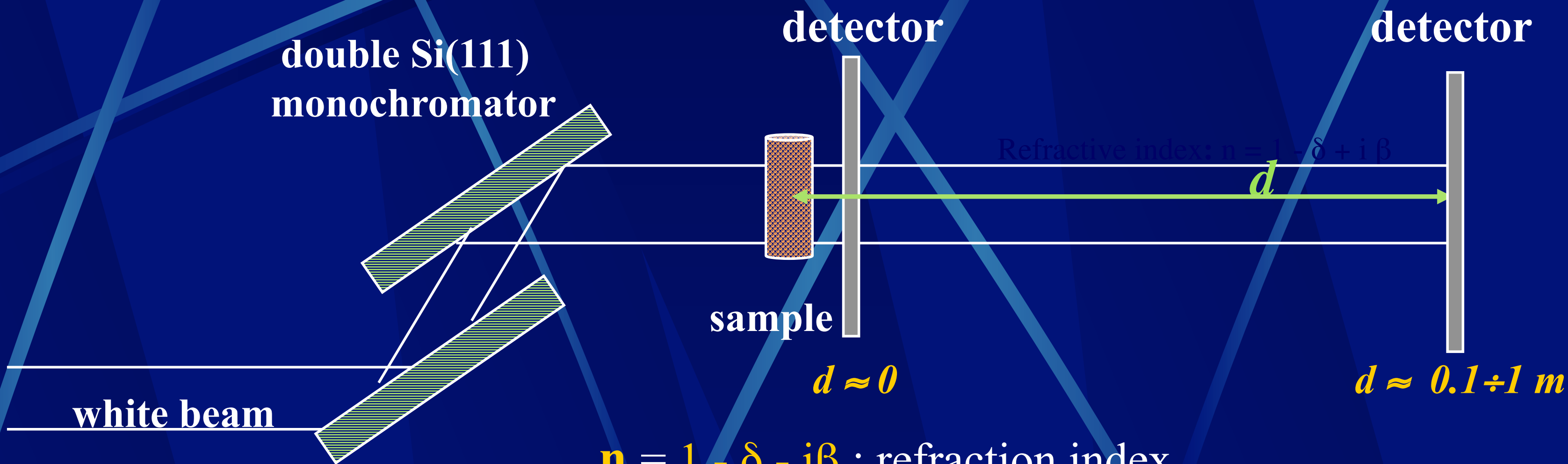

$\mathbf{n} = 1 - \delta - i\beta$: refraction index

$(\Delta I/I)_{abs} = e^{\,c\,\Delta\mu} - 1$

$\mu = 4\pi\,\beta / \lambda$: linear absorption coeff.

c : object size // to beam direction

$\Delta\phi = 2\pi\, c\, \Delta\delta / \lambda$

Fresnel diffraction

$r \ll a \Rightarrow$ *edge detection regime*

$r \cong a \Rightarrow$ *holographic regime*

$r \gg a \Rightarrow$ *Fraunhofer diffraction*

a : object size $\perp$ to beam direction

$r = (\lambda\, d)^{1/2}$: first Fresnel zone radius

Phase vs. amplitude effects with hard X-rays

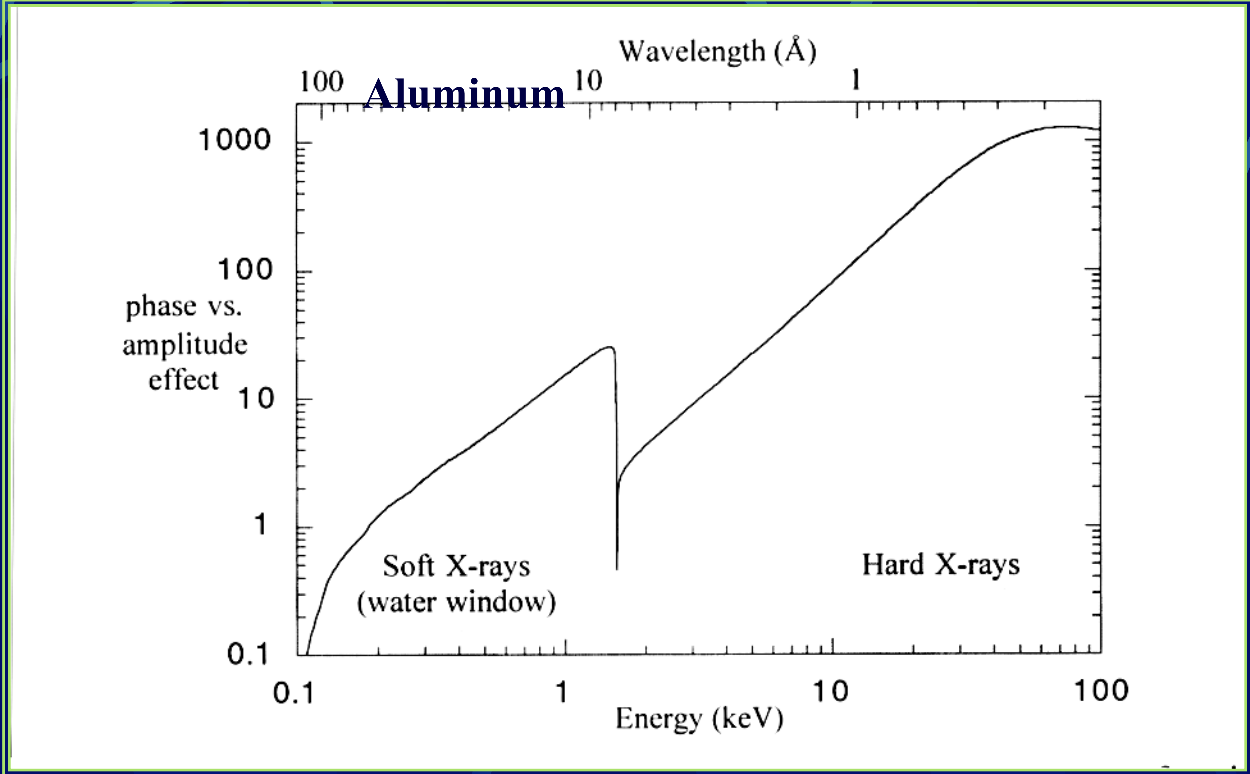

Thus it may be possible to observe phase contrast when absorption contrast is undetectable

Synchrotron Radiation X-Ray Imaging

• Collimation	parallel beams, scatter reduction but fixed spatial resolution
• Monochromaticity	no beam hardening K and L edge imaging quantitative CT evaluations optimization of X-ray energy
• Spatial coherence	phase sensitive techniques
• Intensity	reduction of exposure time but flux decrease at high energies

Digital Subtraction X-Ray Imaging

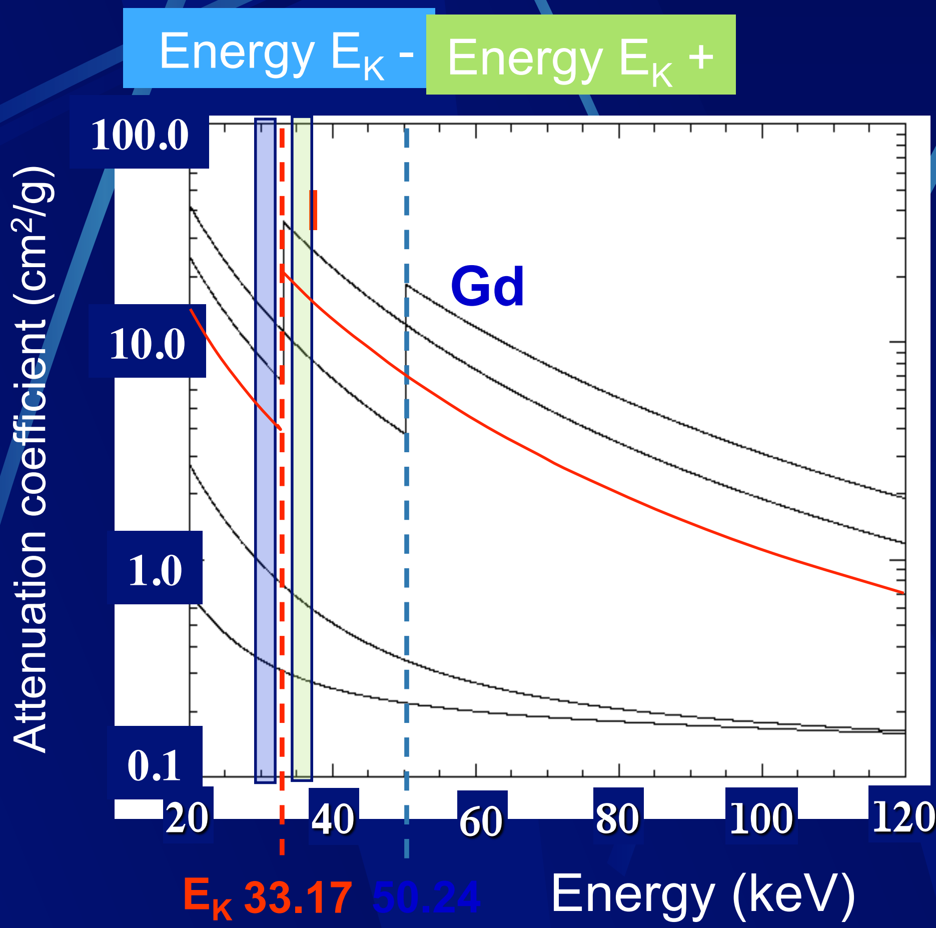

The **atomic scattering factor** contains contributions from **anomalous dispersion** effects which become substantial near the absorption edge of the scattering atom.

$$f = f^0 + \Delta f' + i\Delta f''$$

In medical digital subtraction radiology typical contrast agents are **Iodine** or **Gadolinium**.

Digital Subtraction X-Ray Imaging

$$X_i = \frac{\mu_{Bi} \ln(A) - \mu_{Ai} \ln(B)}{\mu_{Bi}\, \mu_{At} - \mu_{Ai}\, \mu_{Bt}}$$

$$X_t = \frac{\mu_{Bi} \ln(A) - \mu_{Ai} \ln(B)}{\mu_{Bi}\, \mu_{At} + \mu_{Ai}\, \mu_{Bt}}$$

Below Above K-edge

Iodine Image

Two Images are acquired : Above (A) and Below (B) the K-edge

Digital subtraction imaging cannot reach the spatial resolution level of fluorescence techniques (XRF or EPMA), but is an important non-destructive complementary tool.

Absorption X-Ray Imaging

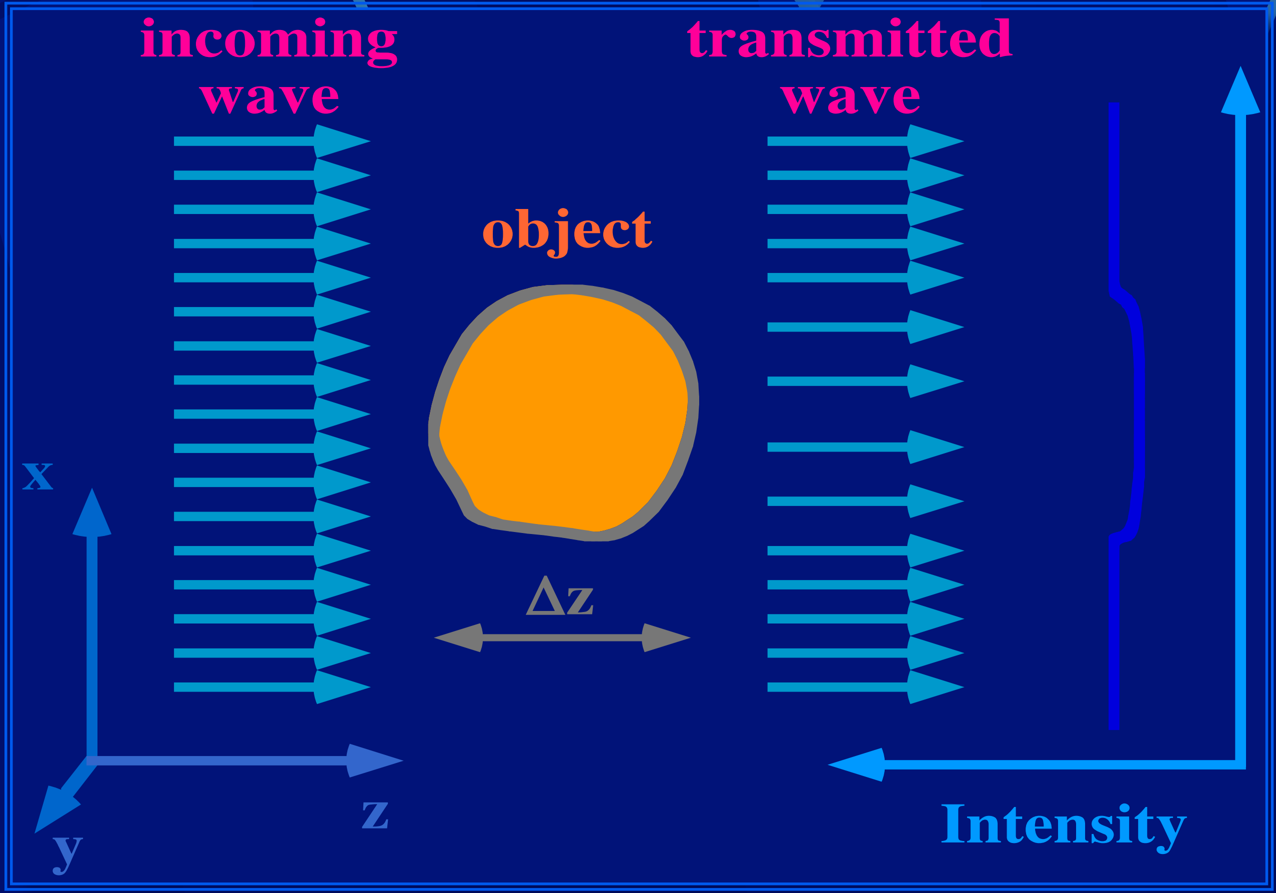

Phase-Contrast X-Ray Imaging

Conventional radiology relies on X-ray absorption as the unique source of contrast and is based exclusively on the detection of amplitude variation of the transmitted X-rays
The main limitation is a poor contrast for samples with low-Z composition or small density variations.

Phase sensitive imaging techniques are based on the observation of the **phase shifts** produced by the object on the incoming wave.

Refractive index: $n = 1 - \delta + i\,\beta$
β = absorption term; δ = phase shift term
$\beta \sim 10^{-10}$; $\delta \sim 10^{-6}$ in soft tissue @ 17 keV
$\delta \propto \lambda^2$, $\beta \propto \lambda^3$
Absorption radiology -> contrast generated by differences in the x-ray absorption ($\beta\,\Delta z$)
Phase Radiology –> contrast generated by phase shifts
$\delta \gg \beta$ –> phase contrast >> absorption contrast

Phase-Contrast X-Ray Imaging

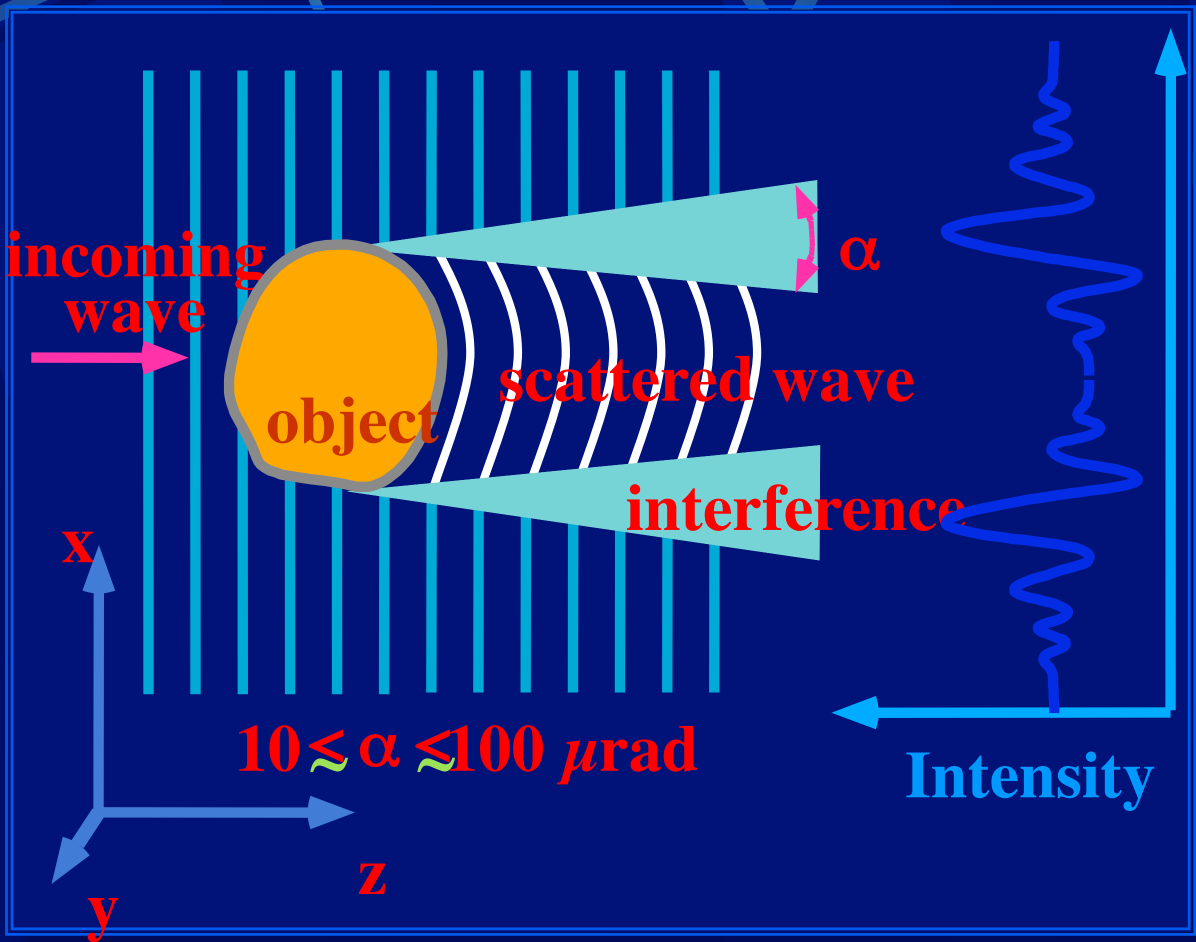

Phase-contrast and absorption

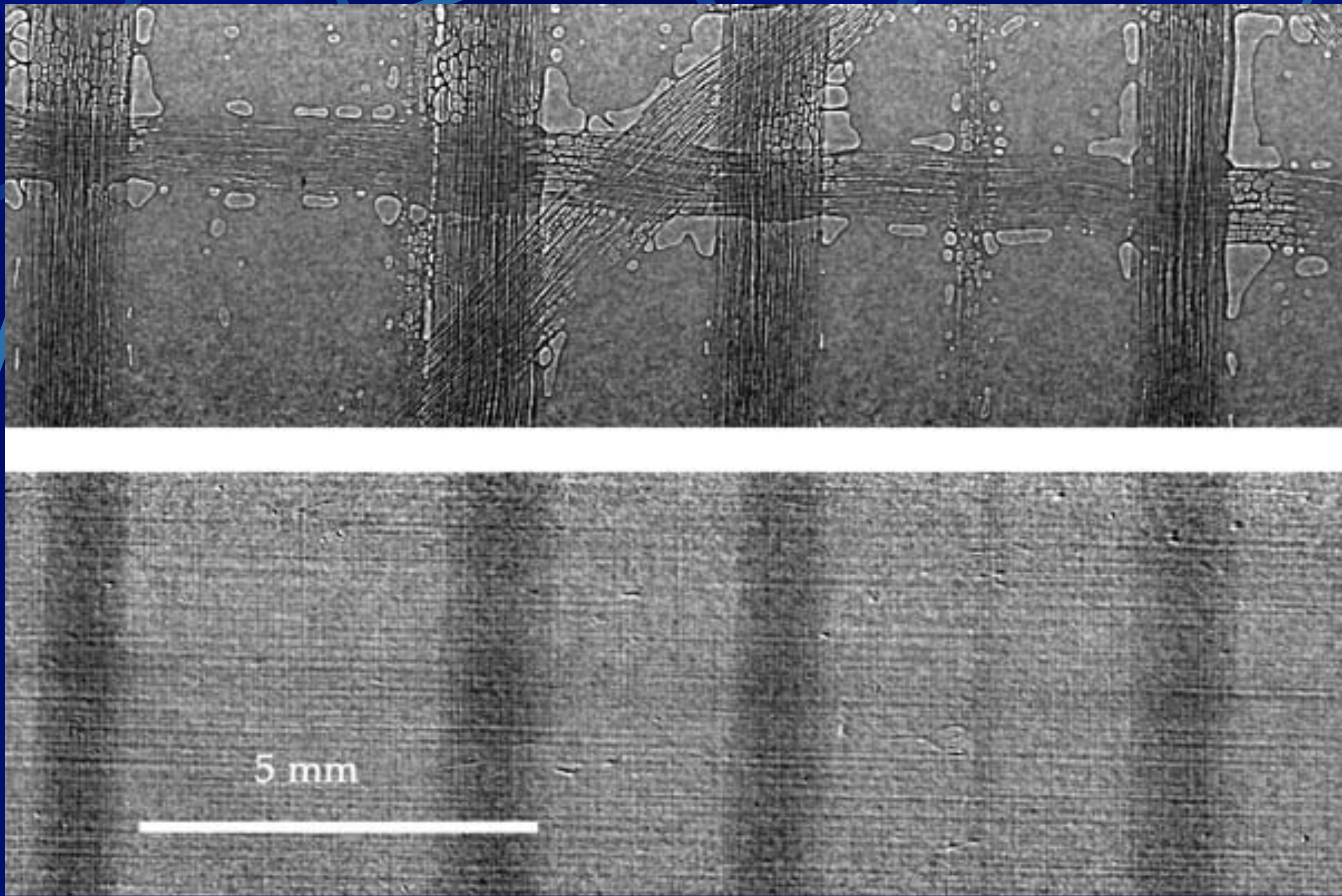

Diax 70 HMT E = 15 keV pixel size = 14 mm

Images of a Mimosa flower ***(D. Dreossi & co.)***

@ 10 keV

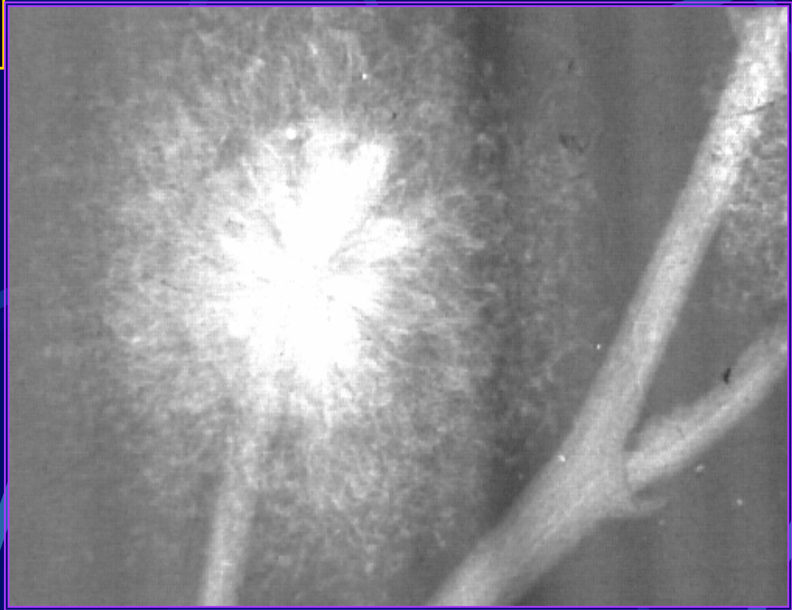

Absorption image

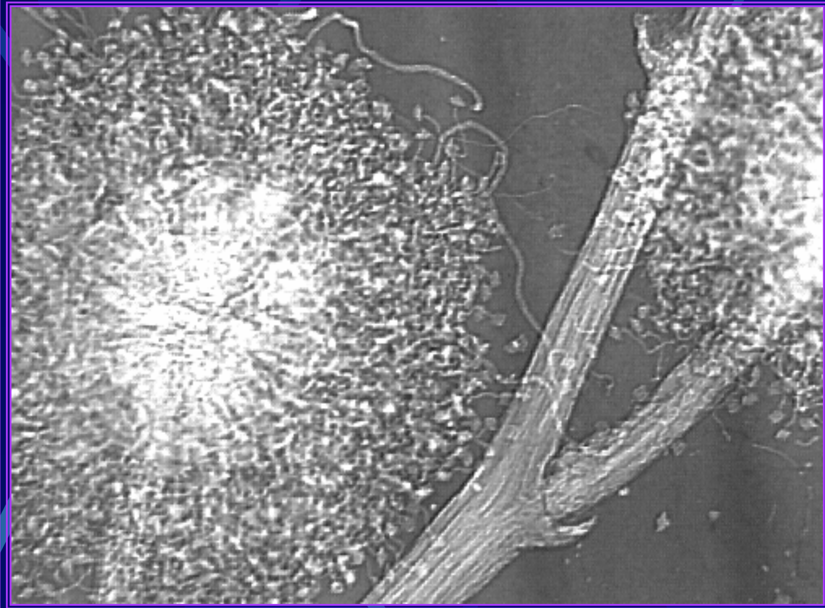

Phase-contrast image

@ 25 keV

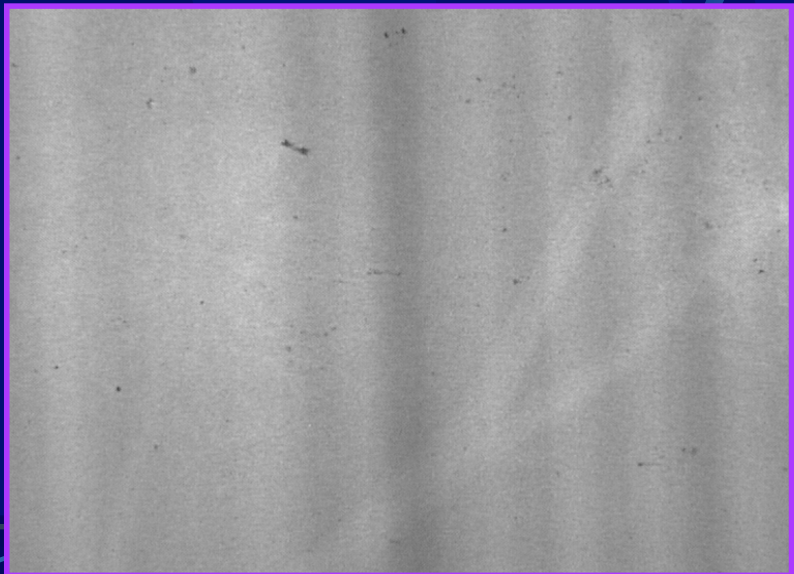

Absorption image

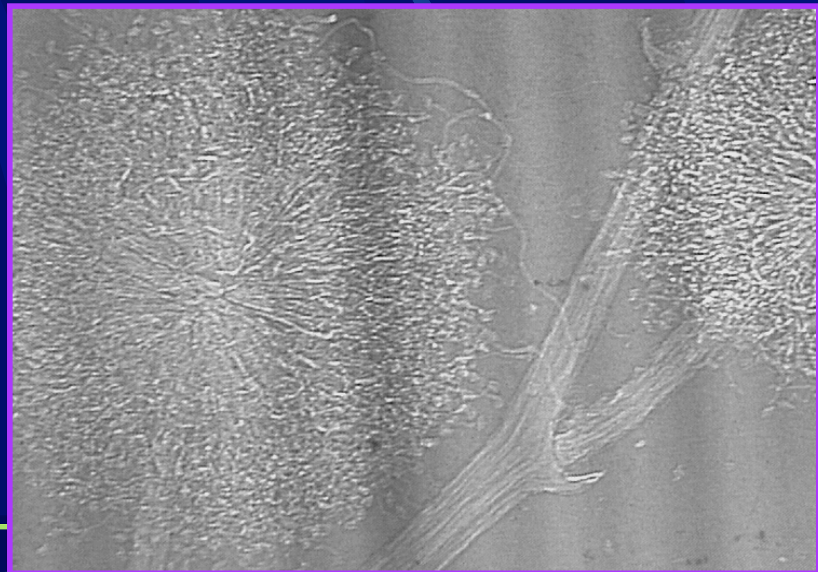

Phase-contrast image

Synchrotron X-ray computed microtomography (μ -CT)

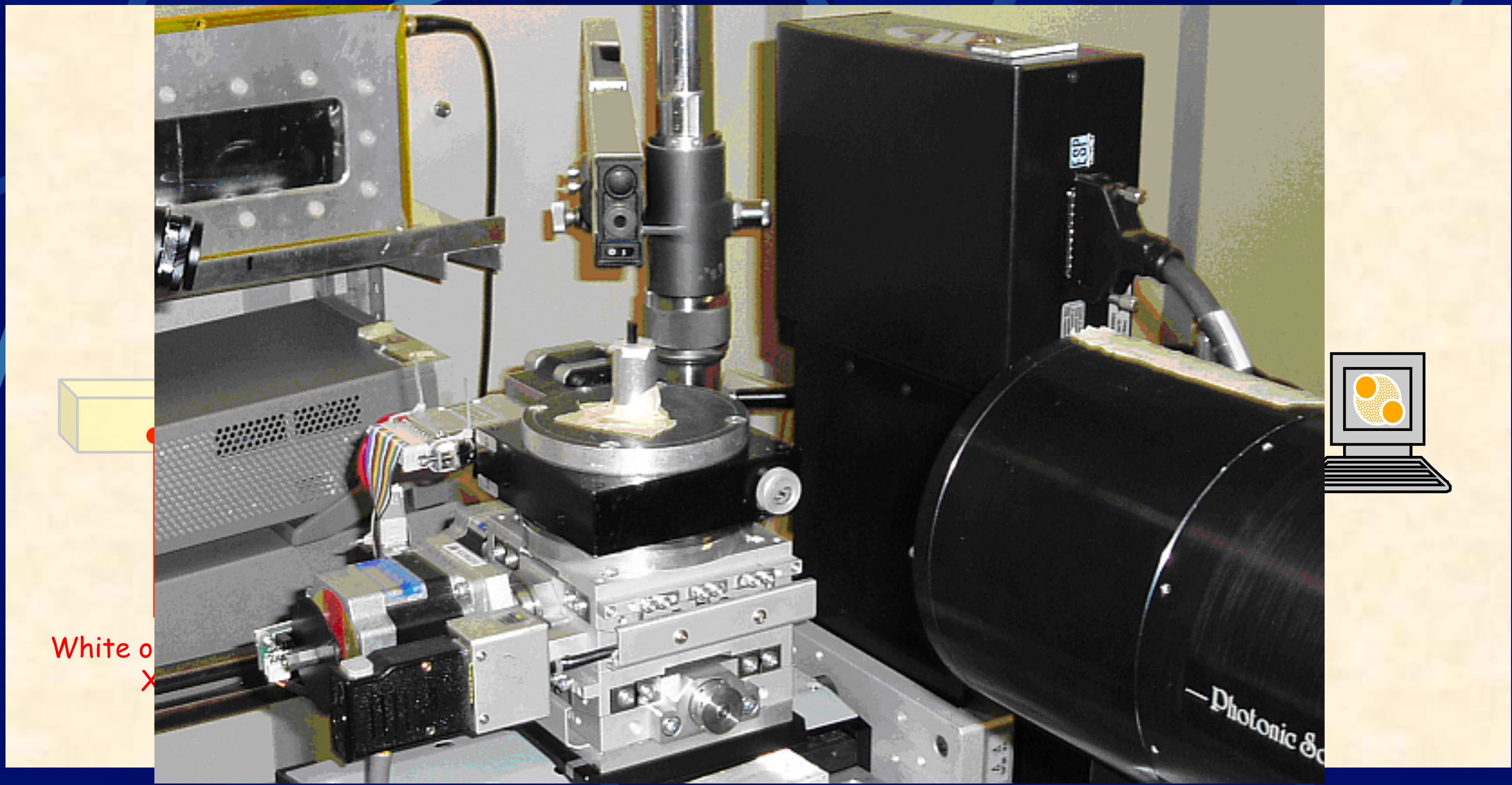

- **Precious** for investigation of **internal features without** sample **sectioning**:
  - → in many cases the **sectioning procedure** modifies the sample structure
  - → the sample can be after **studied by other** experimental **techniques**,
  - → or submitted to several **treatments** (mechanical, thermal, etc...)

CCD detectors & optics

- Photonic Science HYSTAR
  - **16 bit**, **2048 x 2048** pixels^2
  - pixel size: (3.85) 14 x (3.85) 14 μm^2
  - **FOV**: (8) 28 mm x (8) 28 mm
- Photonic Science VHR
  - **12 bit**, **4008 x 2672** pixels^2
  - effective pixel size: 4.5x4.5 μm^2
  - **FOV**: 18 mm x 12 mm

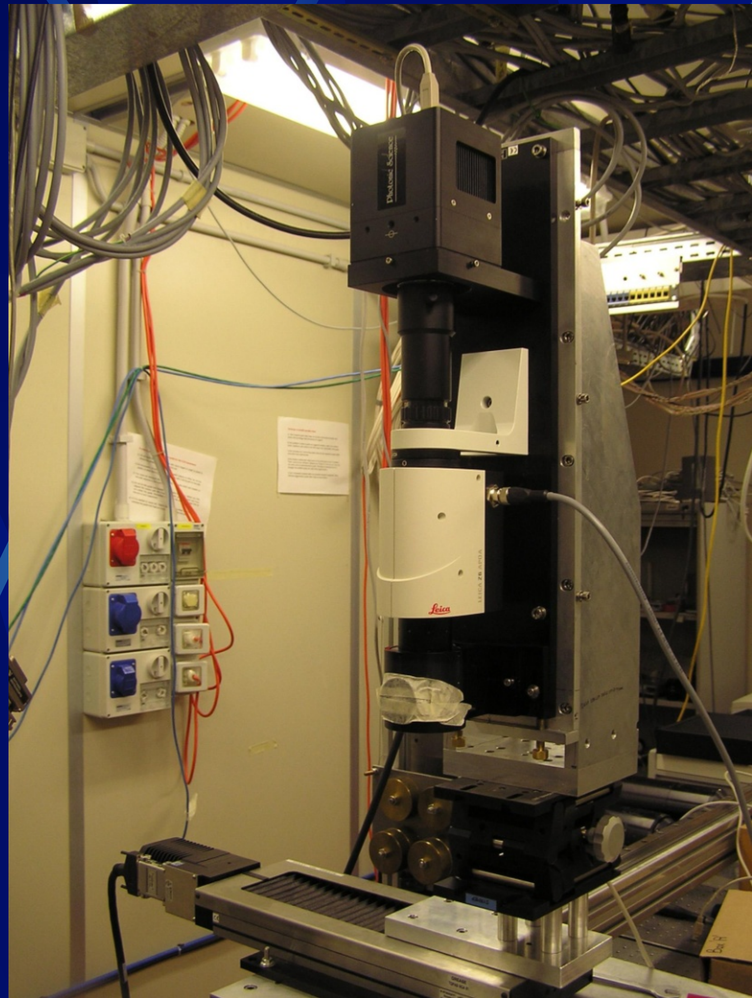

- Photonic Science Lens-coupled
  - **16 bit**, **2048 x 2048** pixels^2
  - pixel size: 7.4x7.4 μm^2
  - **FOV**: continuously adjustable

Optics upgrade: access to white beam for HR imaging

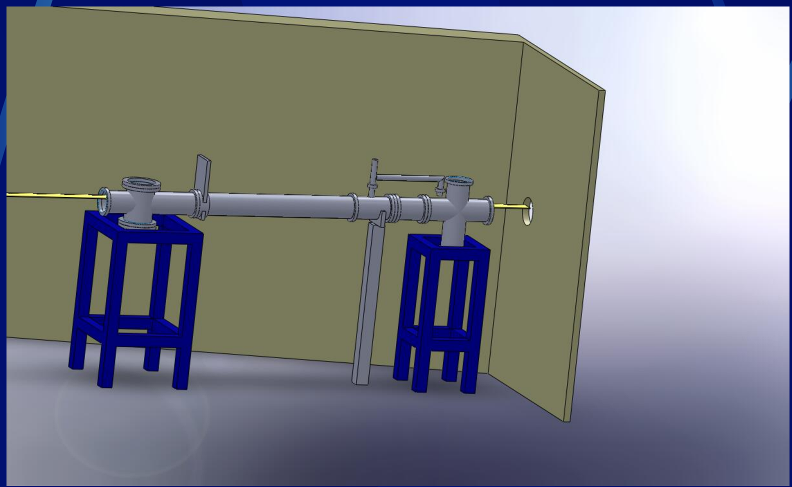

Monochromatic beam mode
(previous set-up)

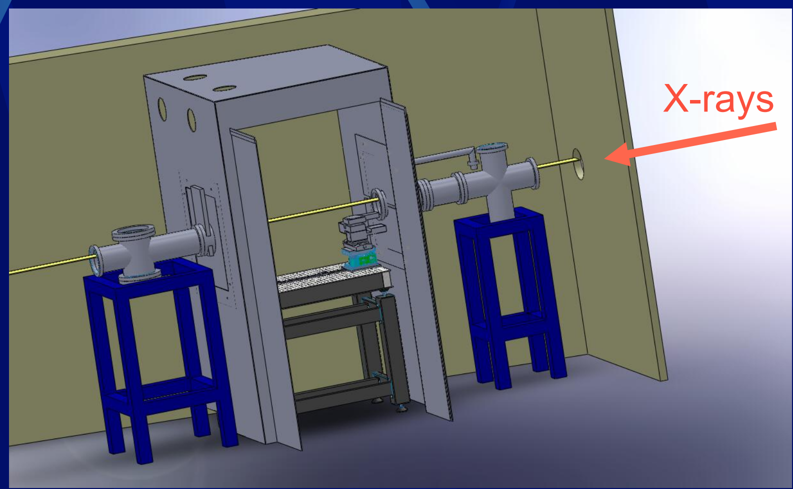

White beam operating mode

TOMOLAB: a conventional μ-CT station at Elettra

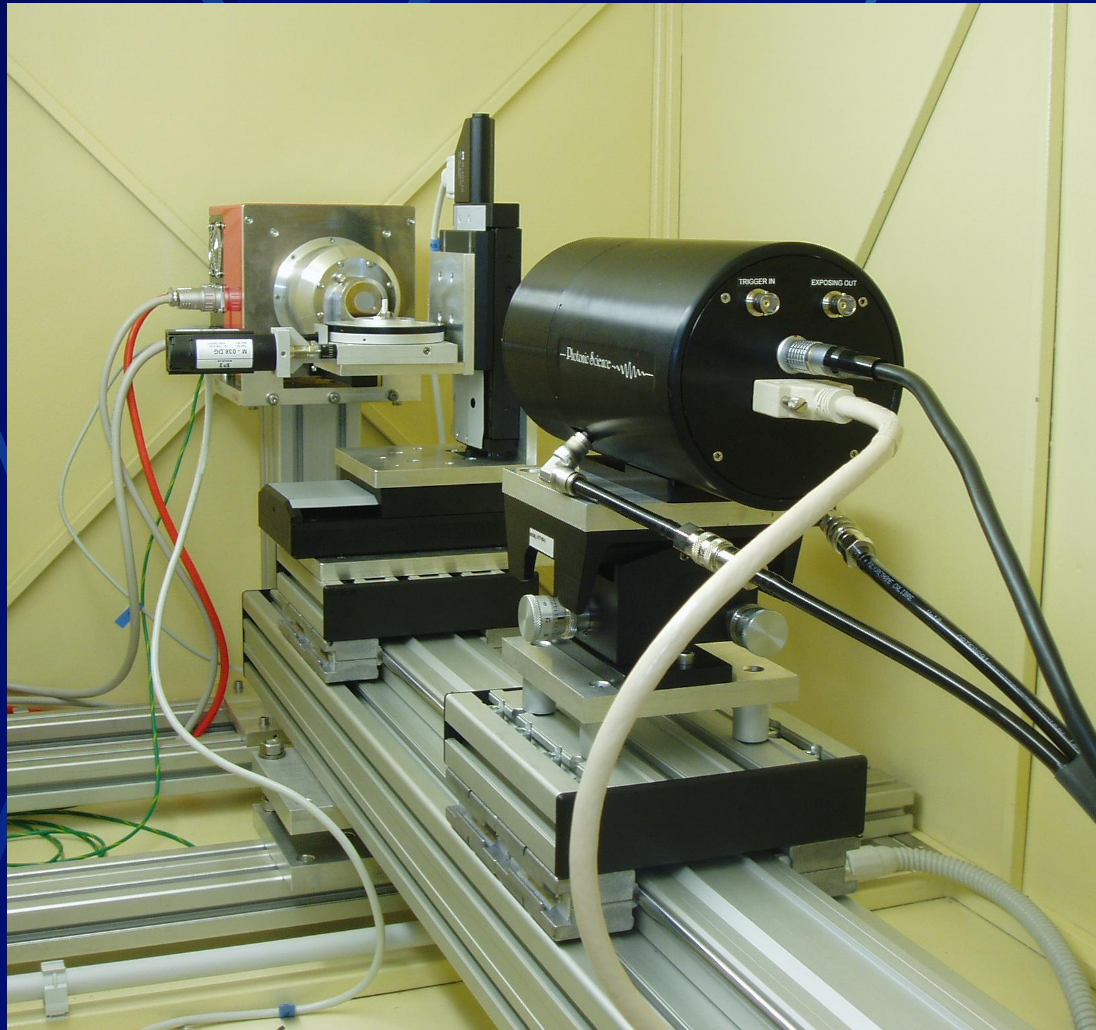

Designed at ***Elettra*** and constructed in collaboration with Georesources Dept. and Corso di Laurea in Odontoiatria e Protesi Dentaria - Facoltà Medicina e Chirurgia of the ***Università of Trieste***.

V = **40÷130 kV**, P_{max} = **39 W**, focal $spot_{min}$ = **5 μm**

Elaboration of tomographic images

- Planar radiographs are elaborated by a **reconstruction procedure**:

  → **filtered backprojection** algorithm *[Herman, 1980]*

  → for each projection an **intensity map** is recorded in the xy detector plane

  → projections are submitted to **filtering procedures**

  → each intensity map is **back projected** along the normal to the projection itself

  → finally, the intensities are added for all the projections

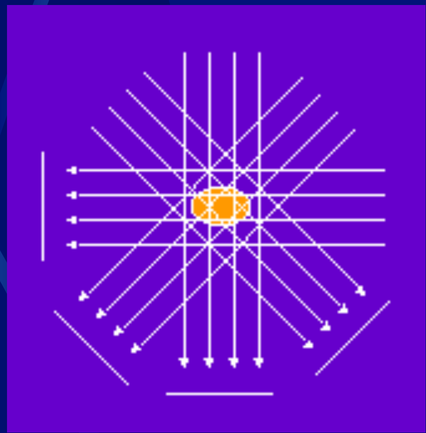

- Reconstructed slices are then treated by a **rendering procedure**:

  → 2D slices visualized as **Stack**

  → 3D views of the sample can be obtained (**Volume rendering**)

- Rendered images can be elaborated applying filters, false colors, **segmentation tools** to extract quantitative information.

Biomaterials

Implanted bone

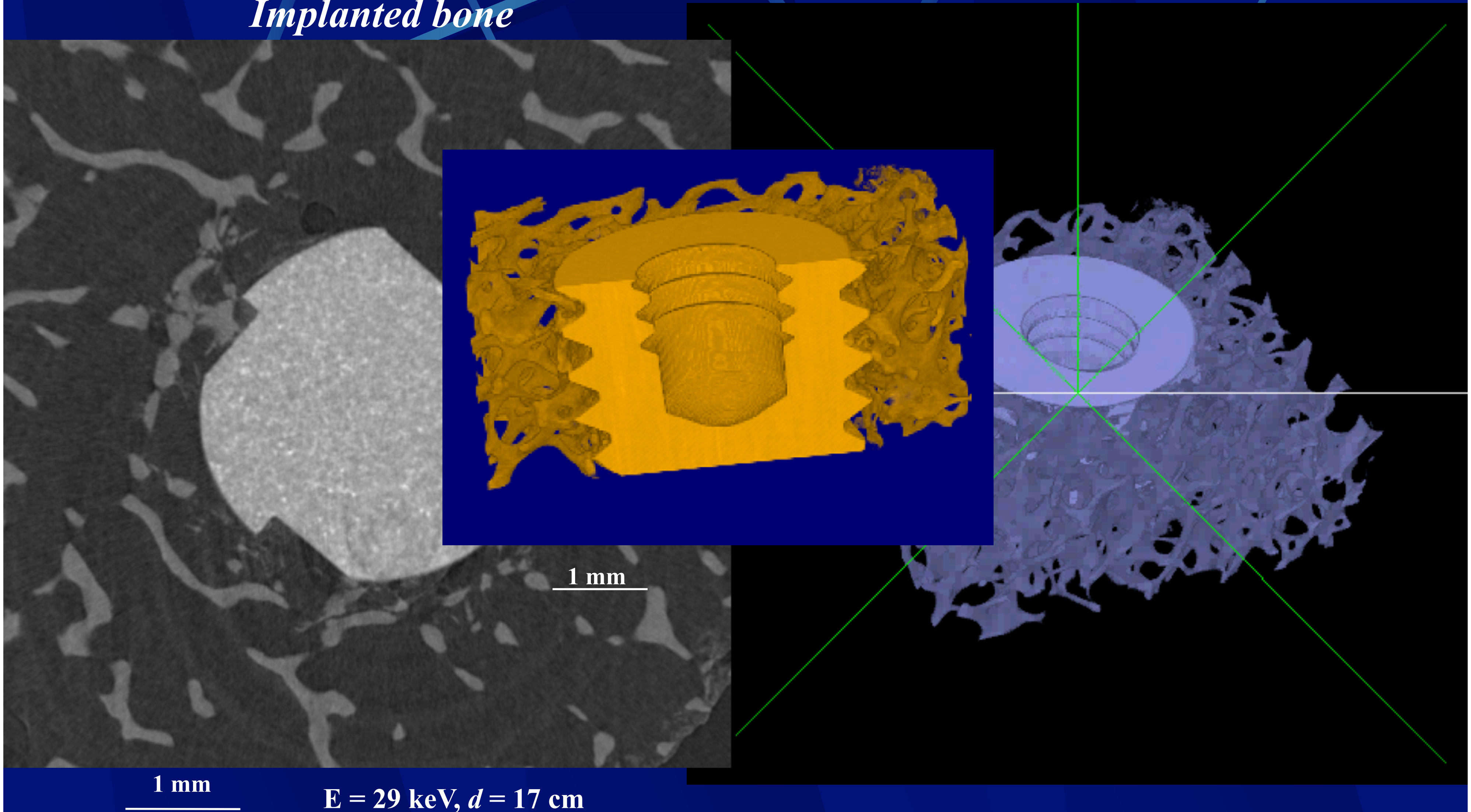

E = 29 keV, d = 17 cm

L. Tesei et al., Nucl. Instrum. and Meth. A, Vol. 548, Issues 1-2 (2005) 257-263.

Food science

Bread crumb

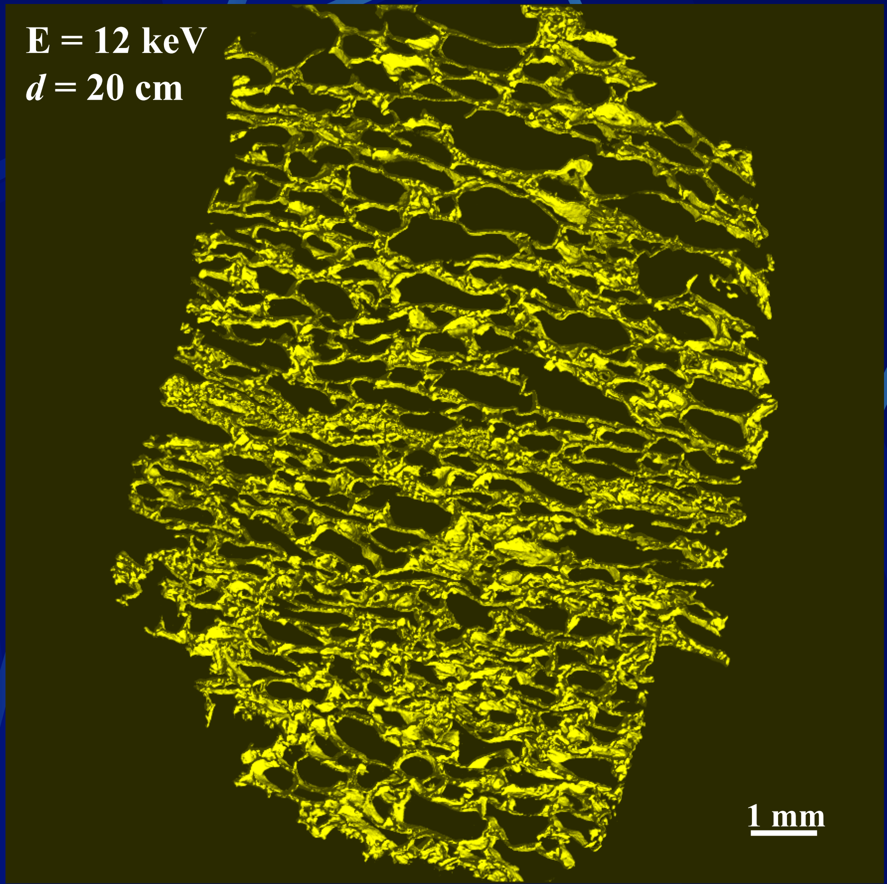

Aerated chocolate

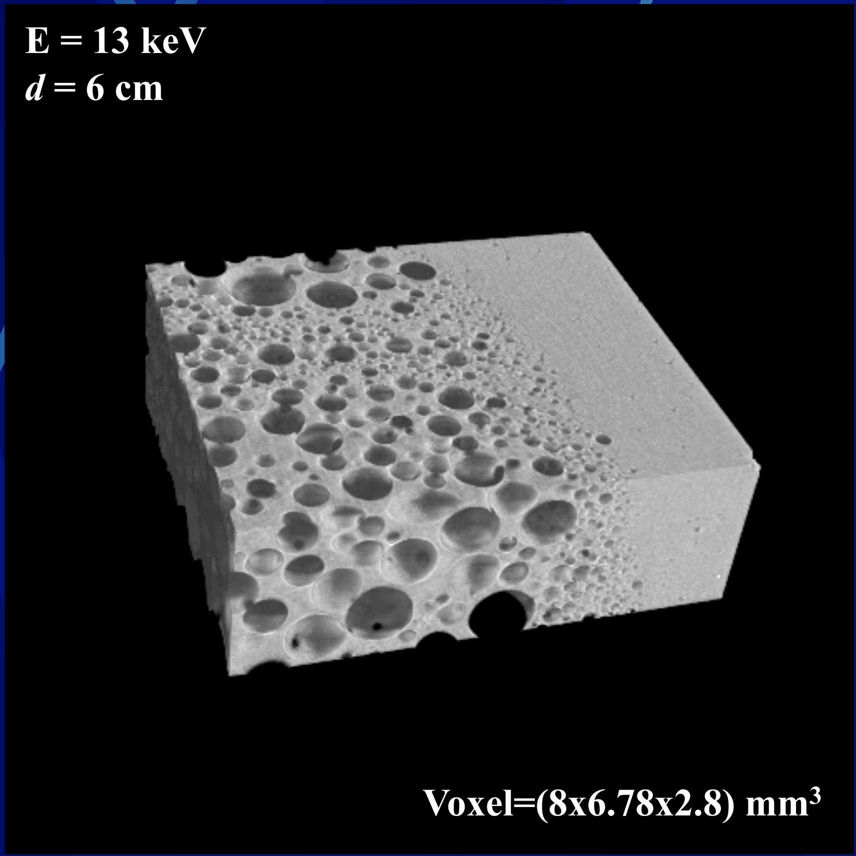

P.M. Falcone et al., Advances in Food and Nutrition Research 51 (2006), 205-263
P. M. Falcone et al., Journal of Food Science 69 (2004) E39-E43

Polymeric foams

Wood samples

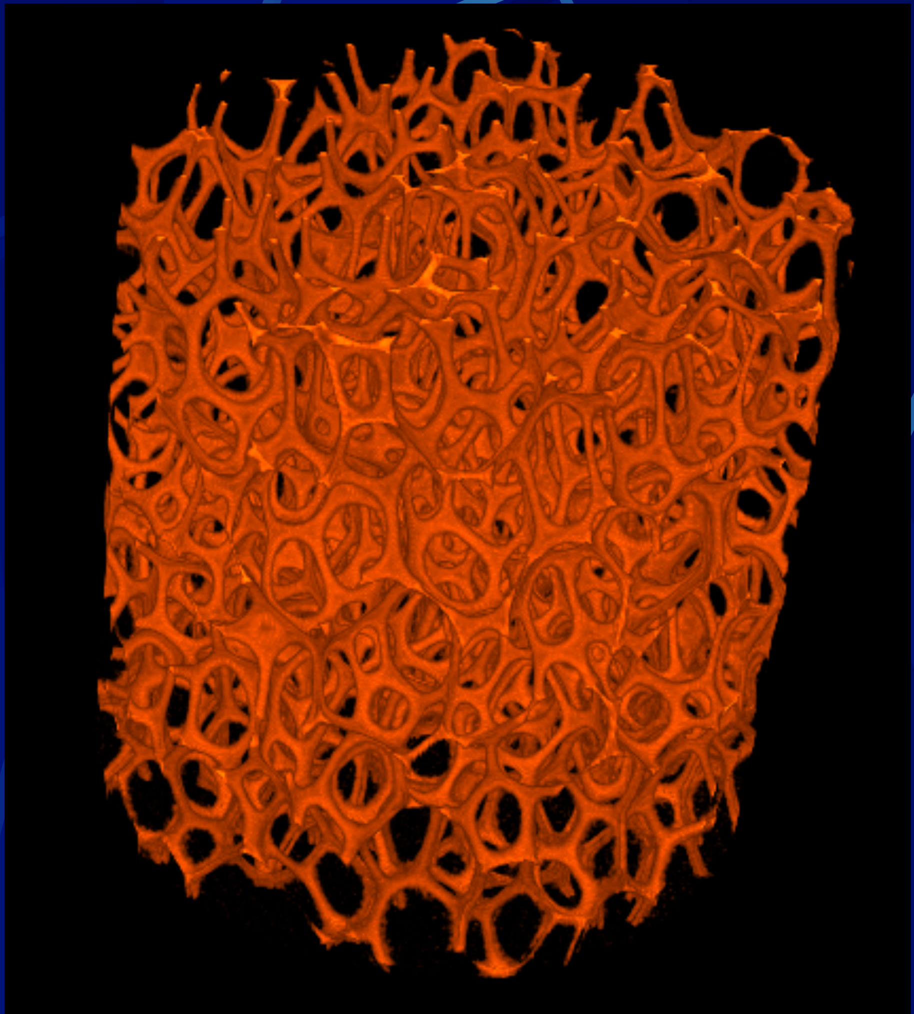

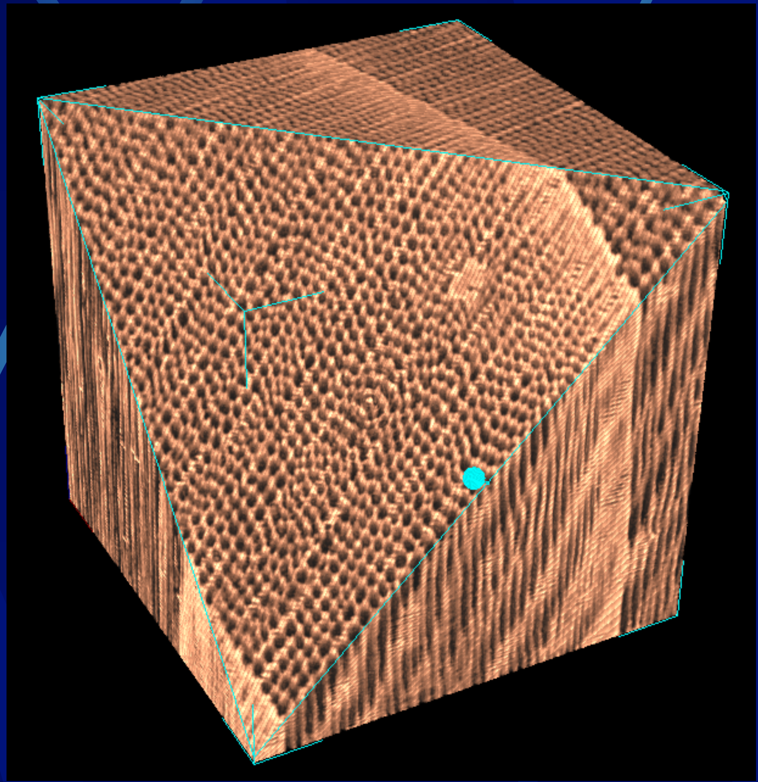

Courtesy of L. Bregant, Univ. of Trieste

D. Dreossi et al., in Wood Science for Conservation of Cultural Heritage - Florence 2007, Firenze University Press 2010, Florence (Italy), pp. 34-39

Kidney stones

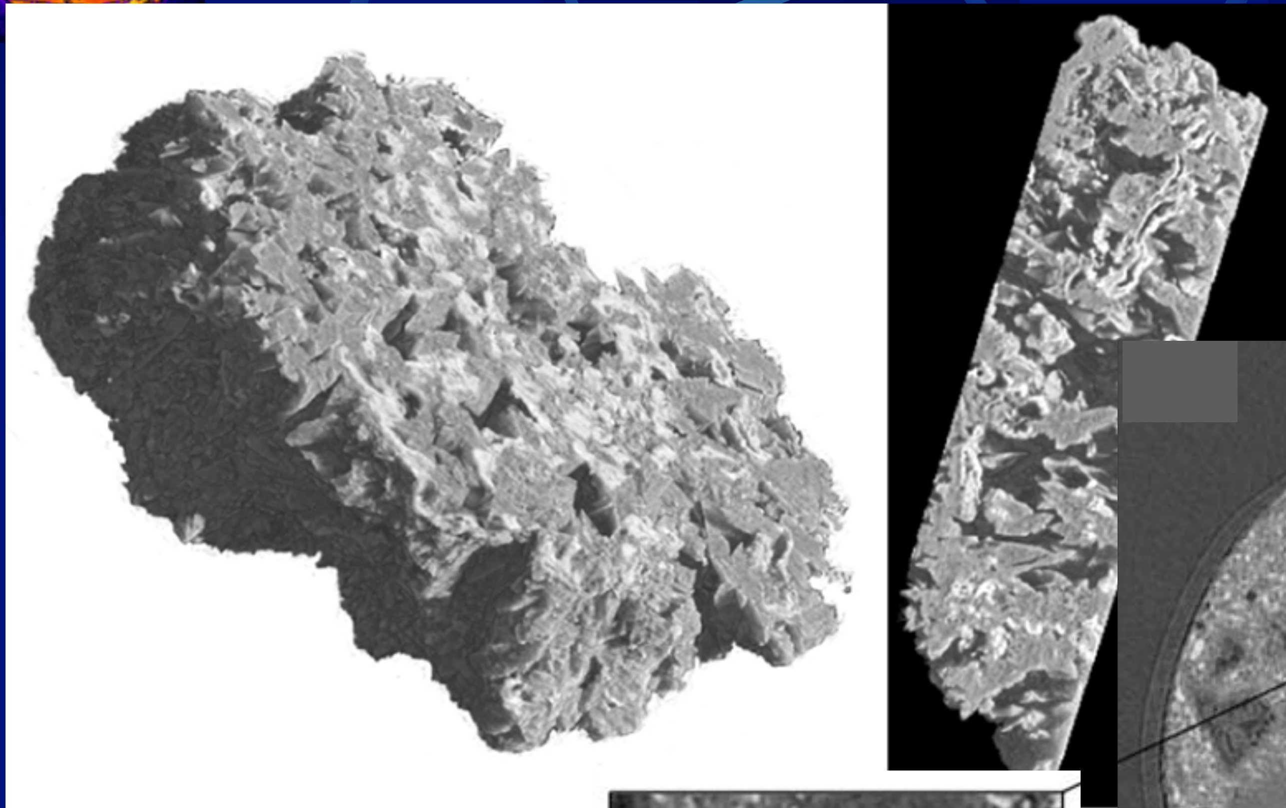

Cement-based materials

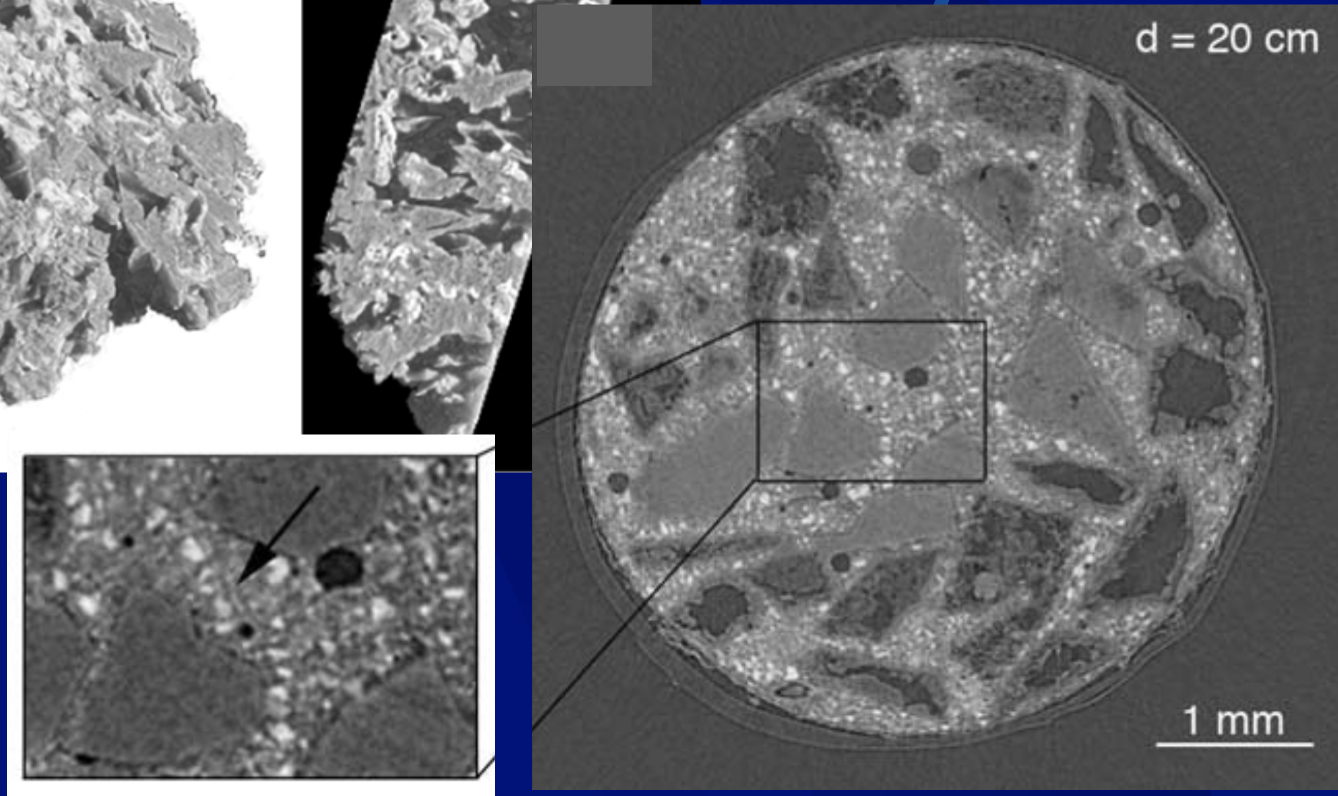

J. Kaiser et al., Urological Research, 39 (2011) 259-267.

N. Marinoni et al., Journal of Material Science, 44 (2009) 5815-5823

Swiss Bee Research Centre

Bee trapped in Amber 20-40 MA old found in the Dominican Republic

E = 14 keV

d = 20 cm

# of proj. = 900

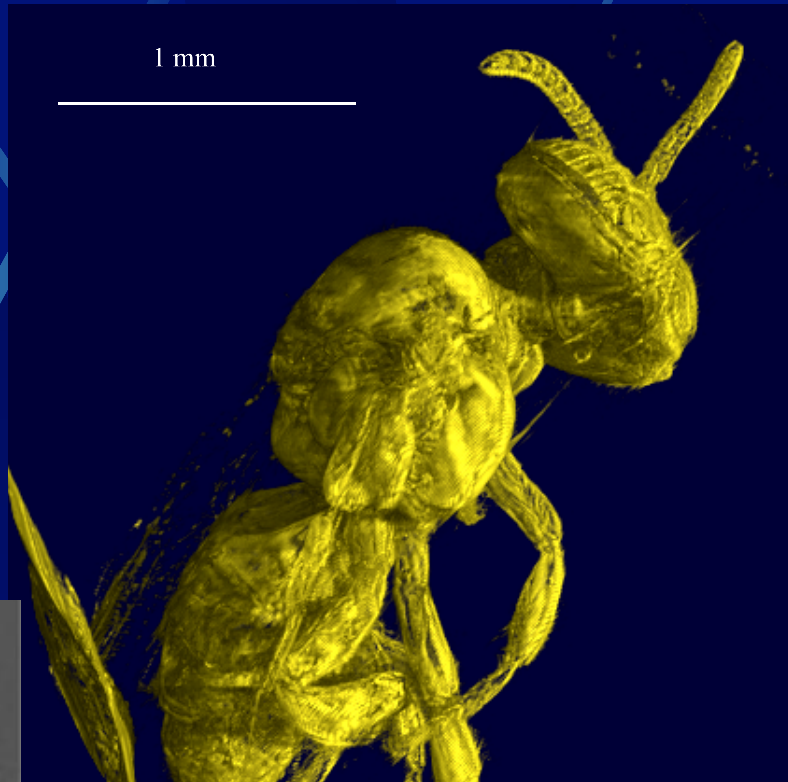

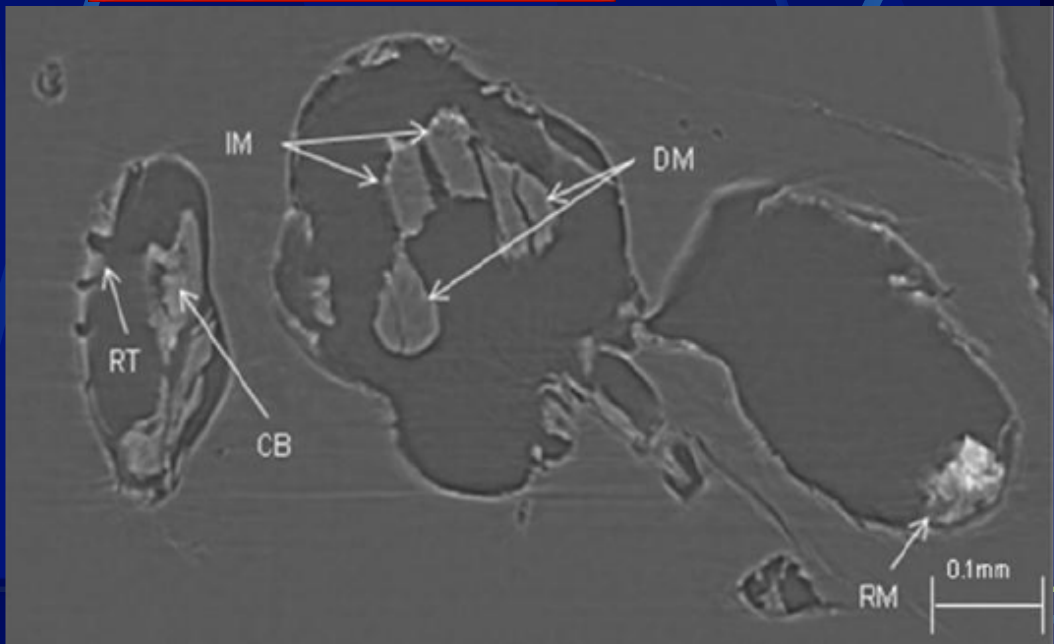

Sagittal view of Proplebeia abdita (Greco and Engel n. sp. holotype)

CB: central body of brain

RT: retinal zone of compound eyes

DM: direct flight muscles

IM: indirect flight muscles

RM: loaded rectum

Greco M.K. et al., Insectes Sociaux (2011), doi: 10.1007/s00040-011-0168-8

Swiss Bee Research Centre

Modern bee: Trigona Carbonaria (stingless Australian bee)

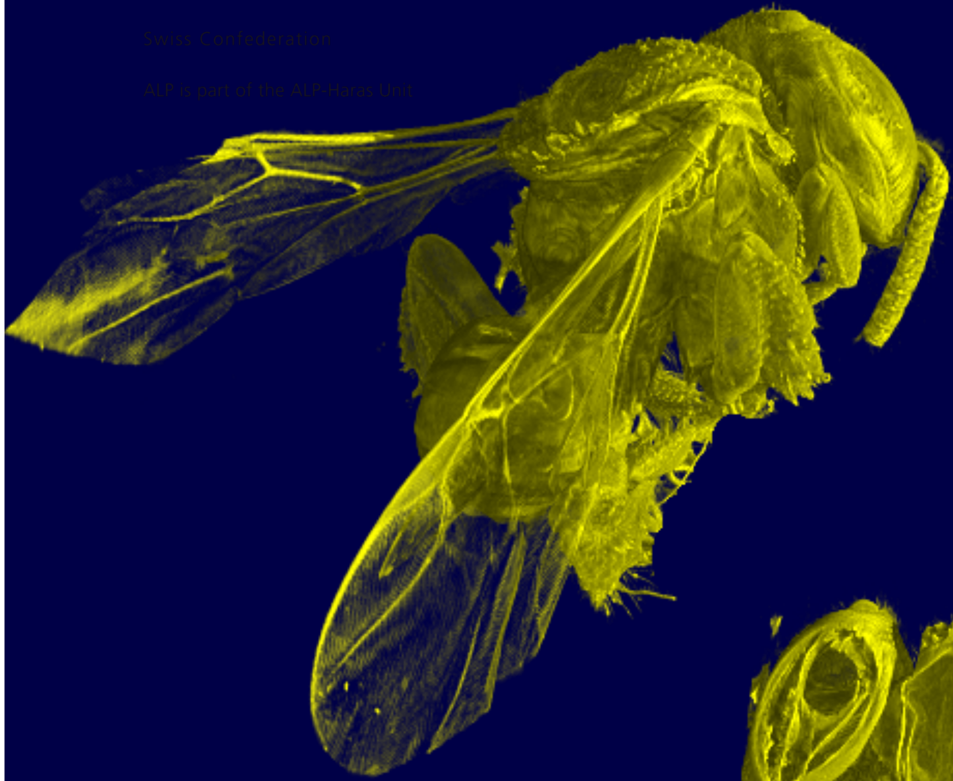

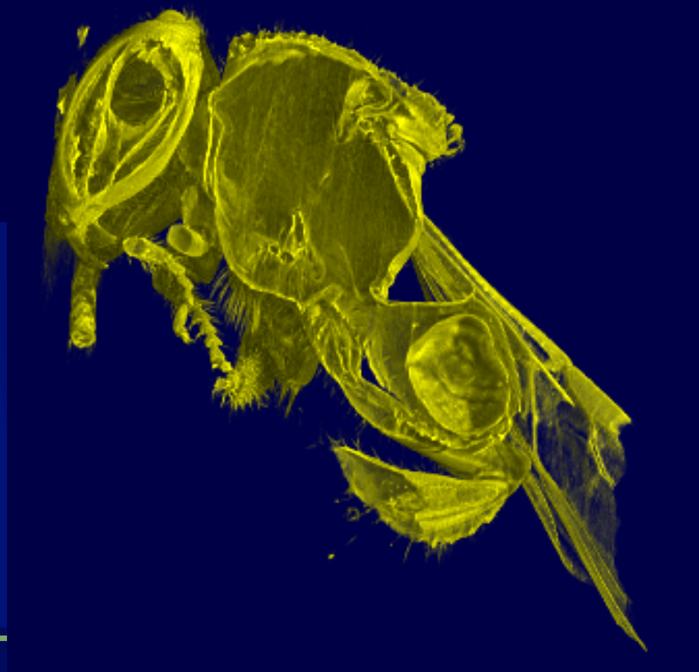

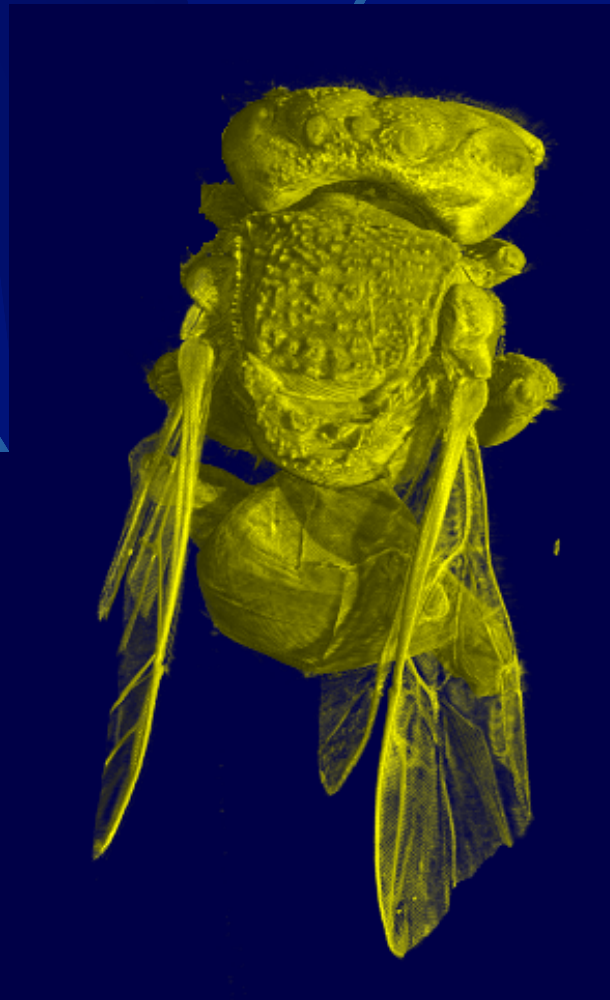

Analysis of a Neanderthal tooth

Volume rendering

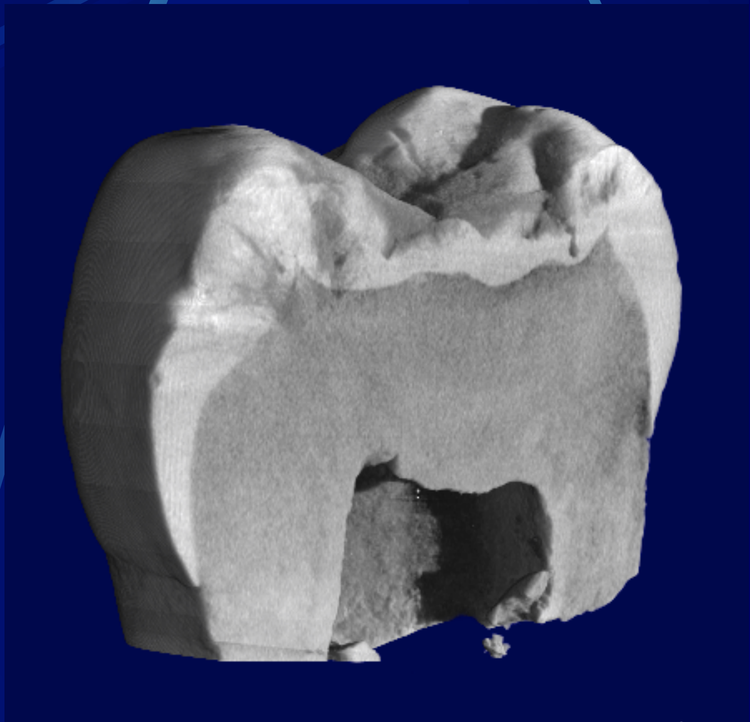

Volume: (1110 x 706 x 946) voxels^3
voxel side = 10 microns

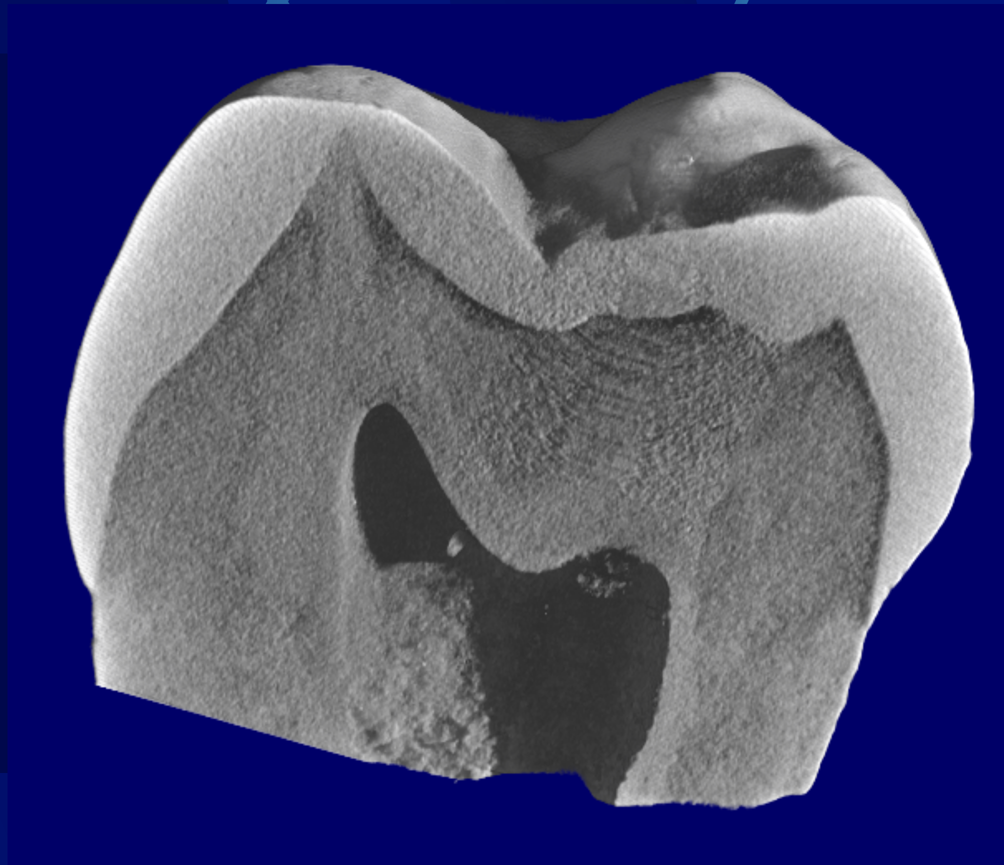

Courtesy of C. Tuniz

BRNO UNIVERSITY OF TECHNOLOGY

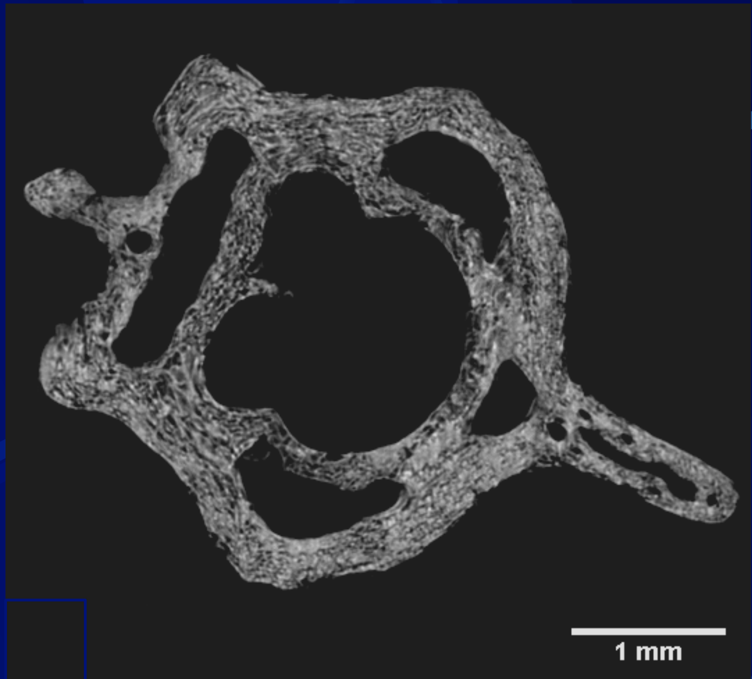

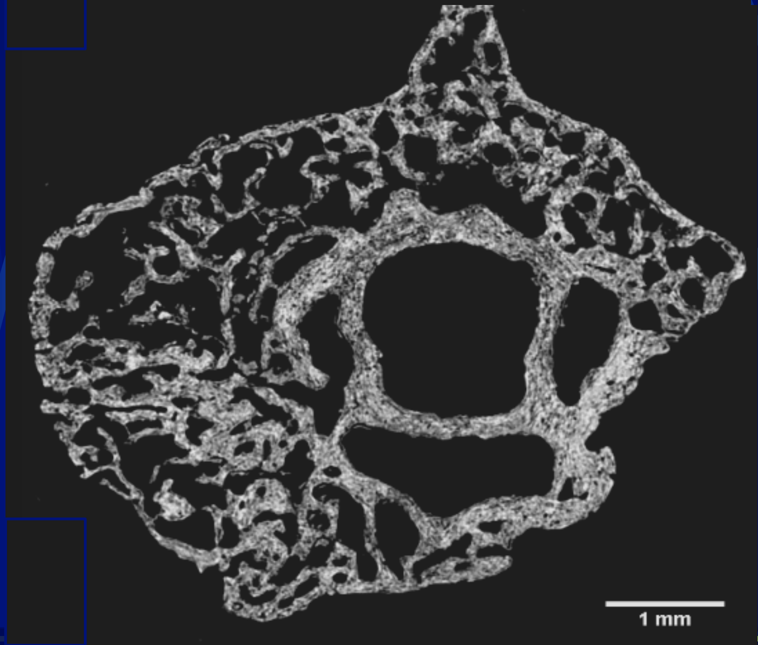

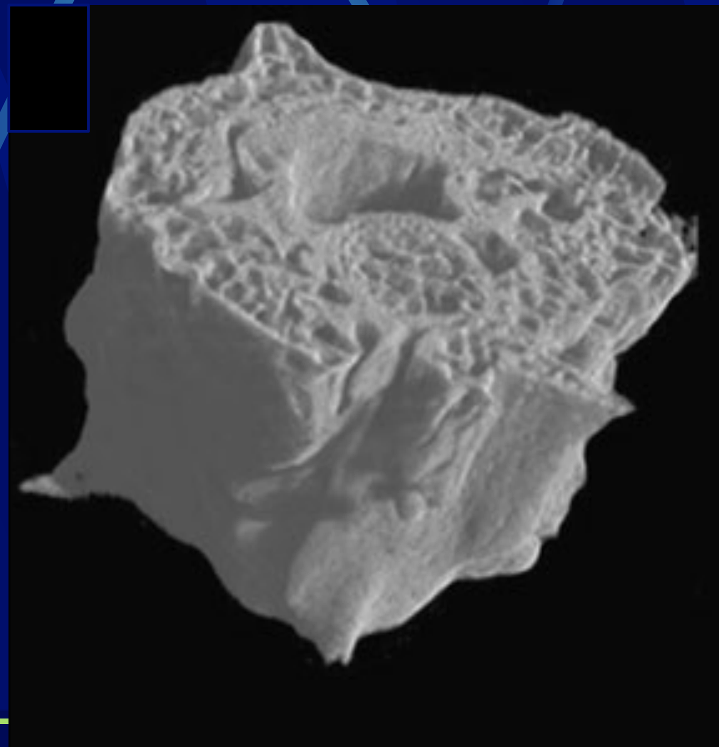

M. Galiová et al., Analytical and Bioanalytical Chemistry, 398 (2010) 1095-1107.

Healthy *Pathological*

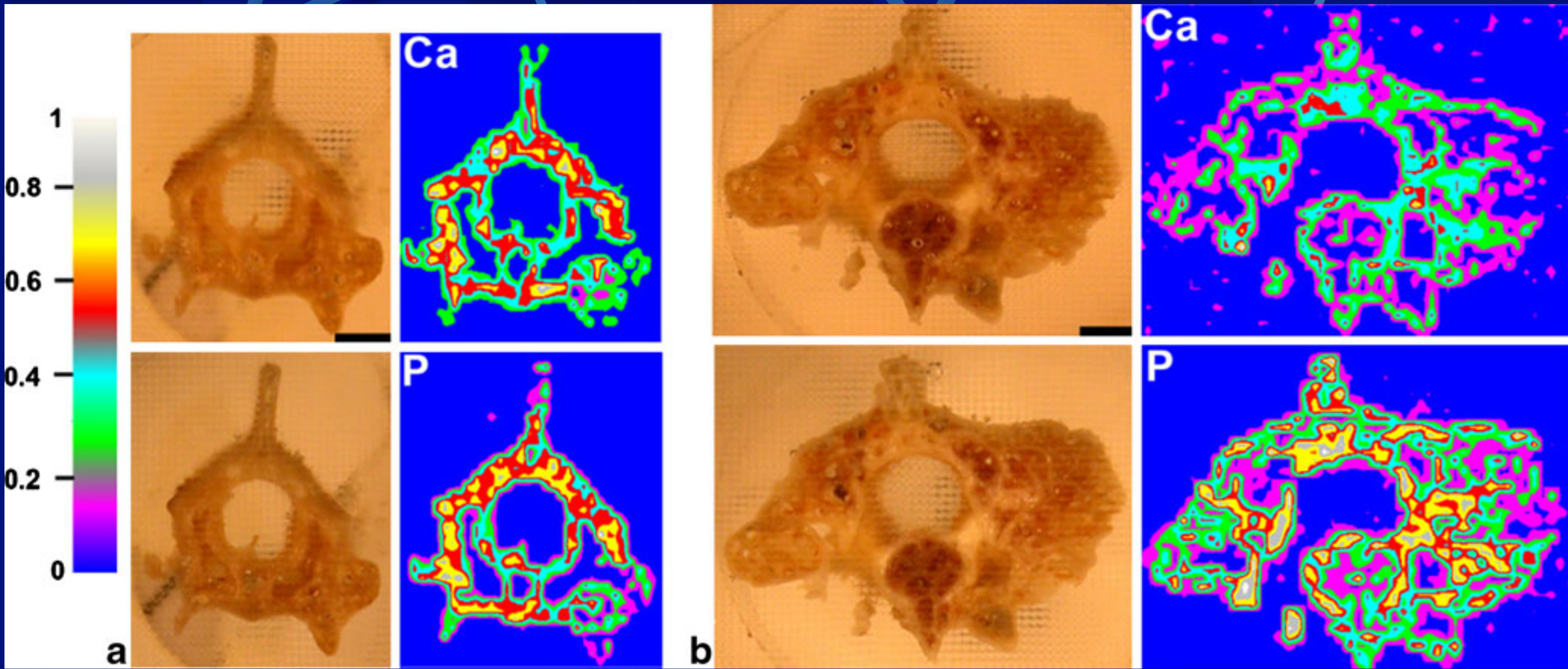

Spatial distribution of trace elements measured on fossil vertebra sections by DP-LIBS technique (bar length = 1 mm)

M. Galiová et al., Analytical and Bioanalytical Chemistry, 398 (2010) 1095-1107.

3D analysis of the canal network of Stylaster sp. (Cnidaria, Hydrozoa) by means of X-ray µCT

Colony *in situ*

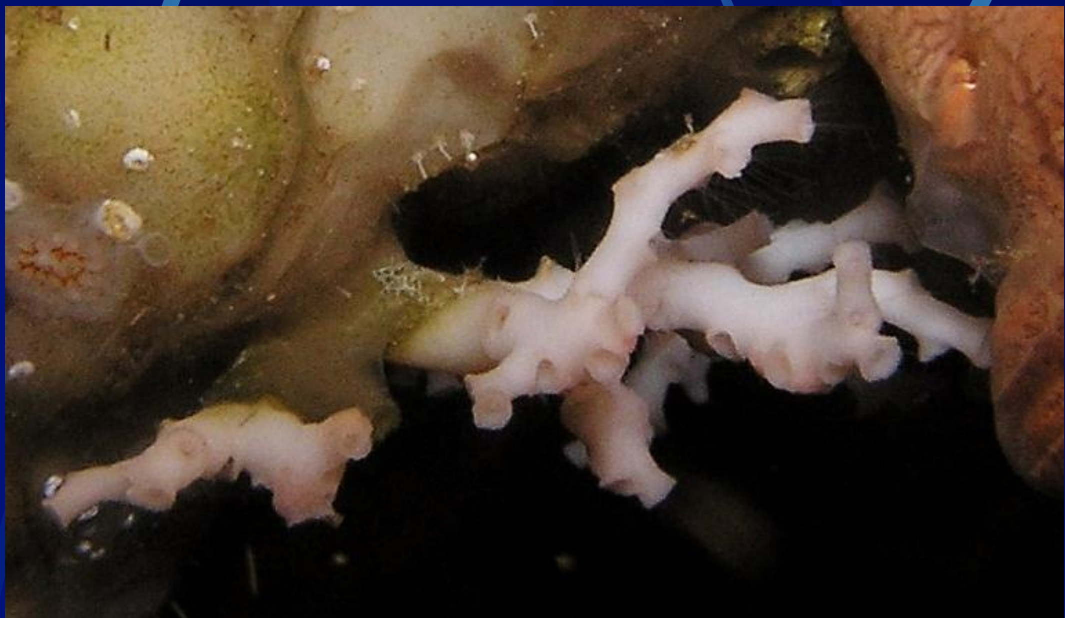

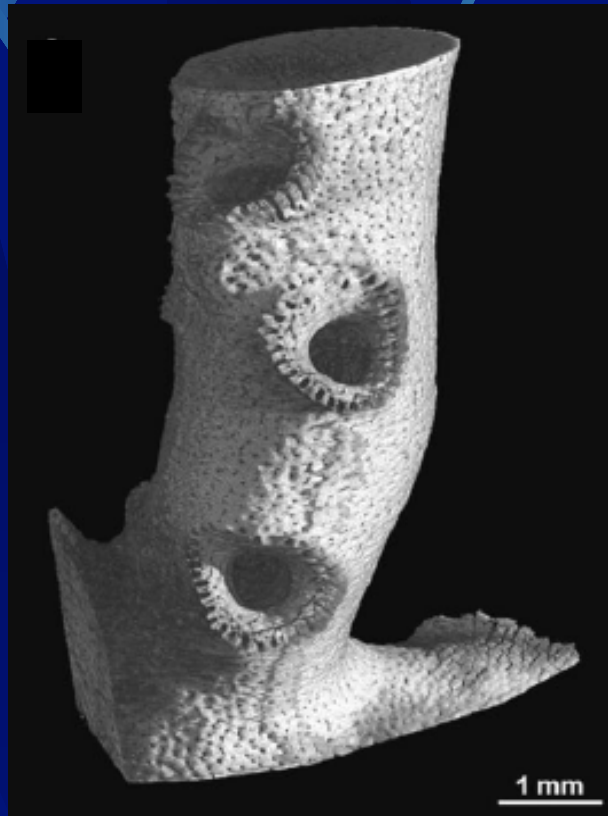

3D rendering of a branch

S. Puce et al., Zoomorphology, 130 (2011) 85-95.

Branch of the colony without coenostem

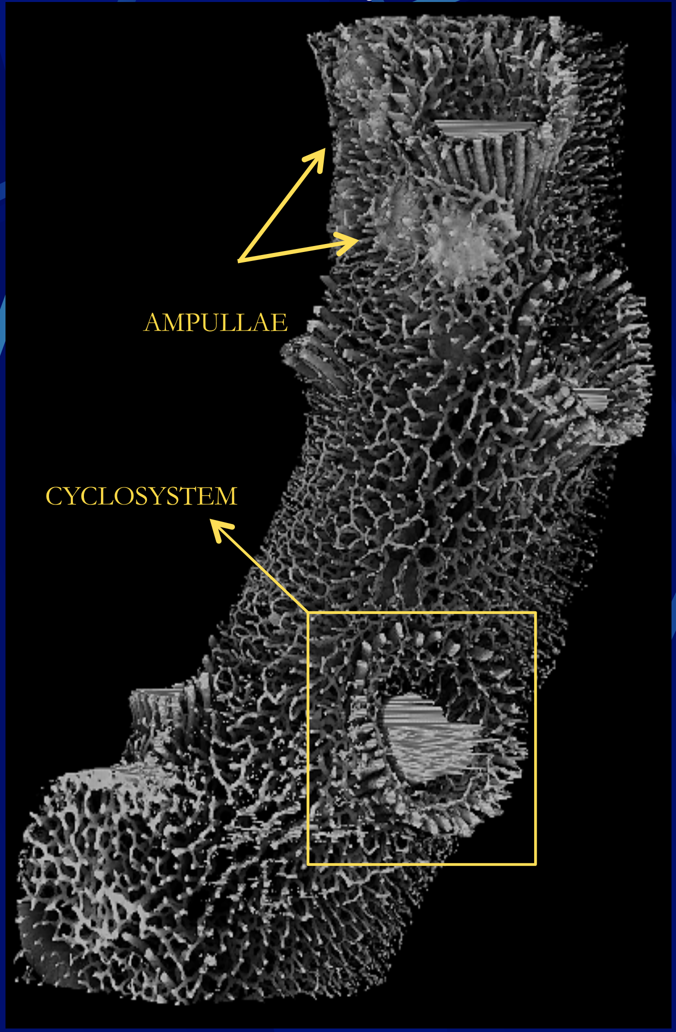

Section of the branch

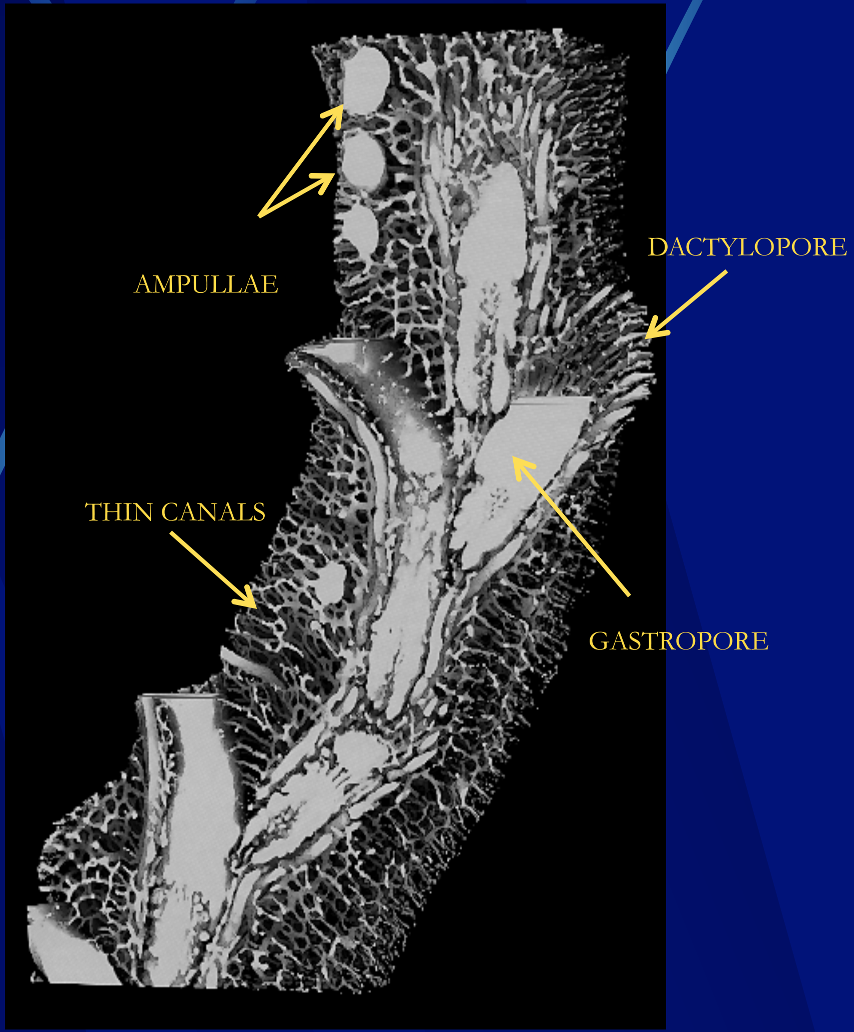

S. Puce et al., Zoomorphology, 130 (2011) 85-95.

Original waterlogged glass, completely corroded

Fragment provided by the Museum of London

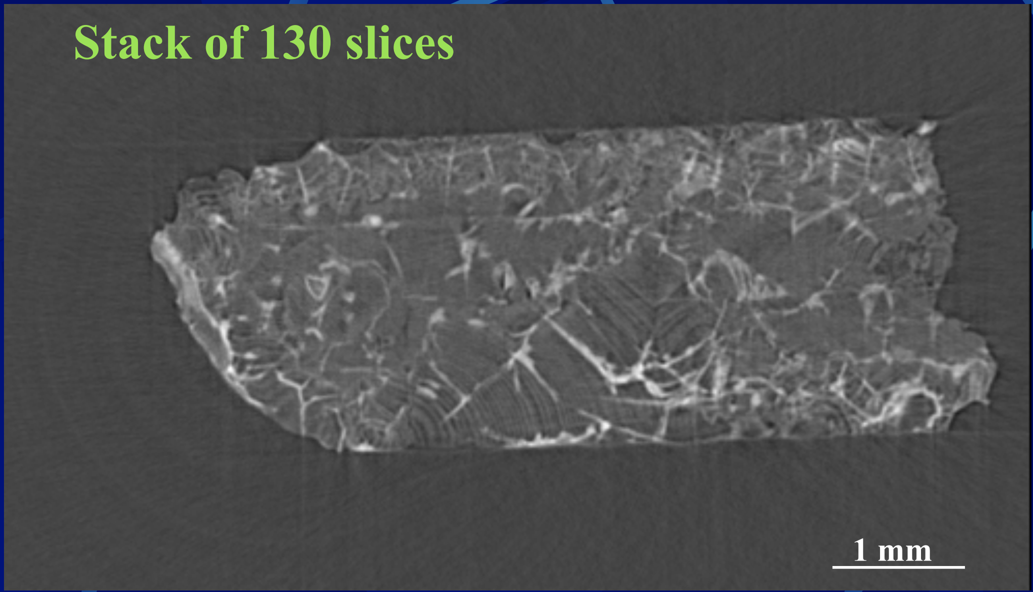

E = 25 keV ***d* = 66 cm;** ***acquisition time: 4h***

It is possible to visualize:

→ the gel-layer channels

→ the lamellar structure inside the corroded glass

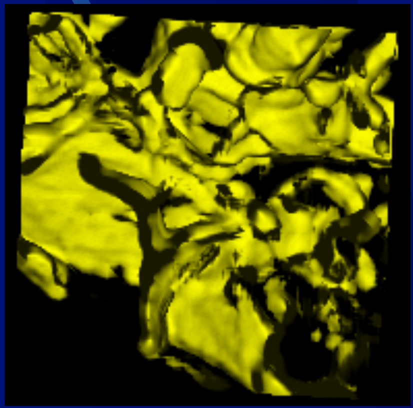

Cine rendering of channels
(9.0 x 9.0 x 0.2) mm^3

L. Mancini et al., Journal of Neutron Research 14, No. 1 (2006) 75–79.

Non-destructive evaluation of musical instruments

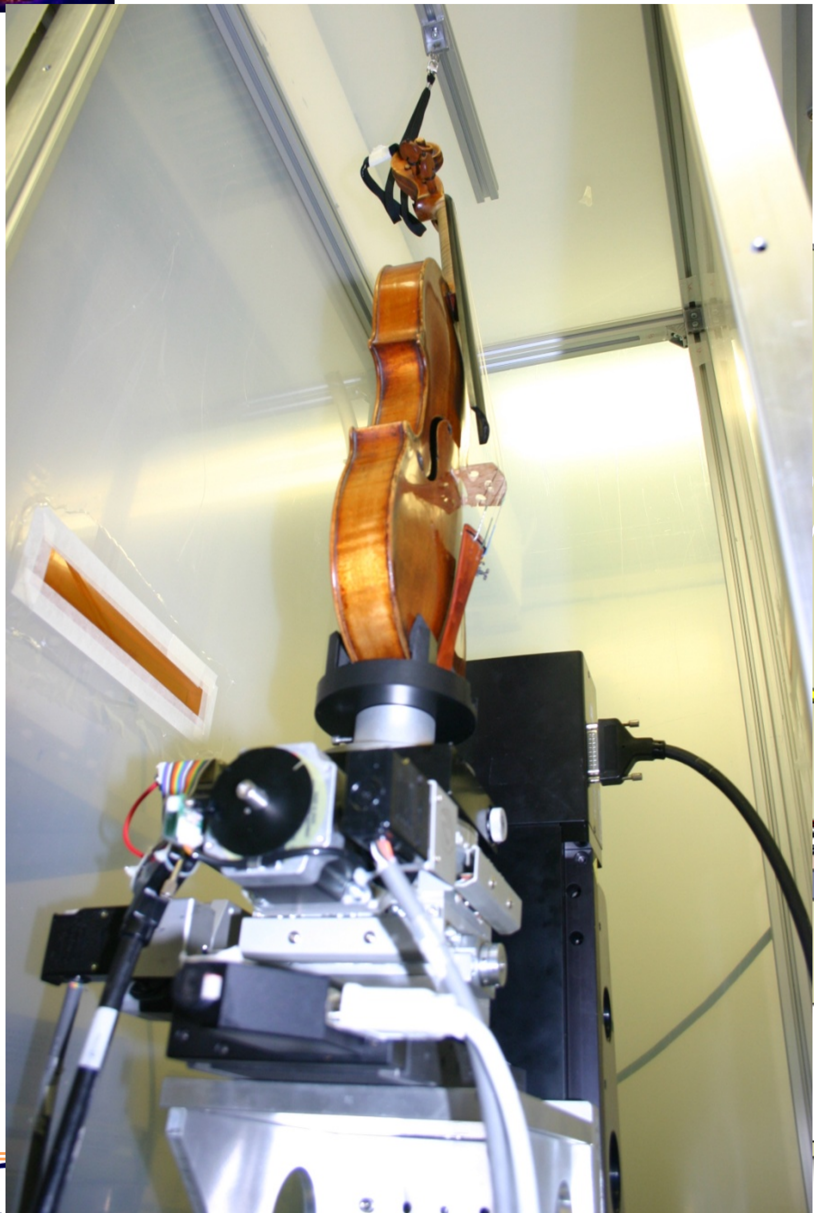

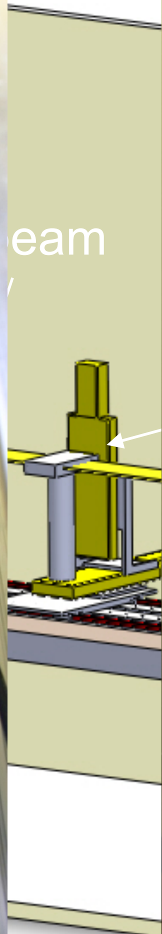

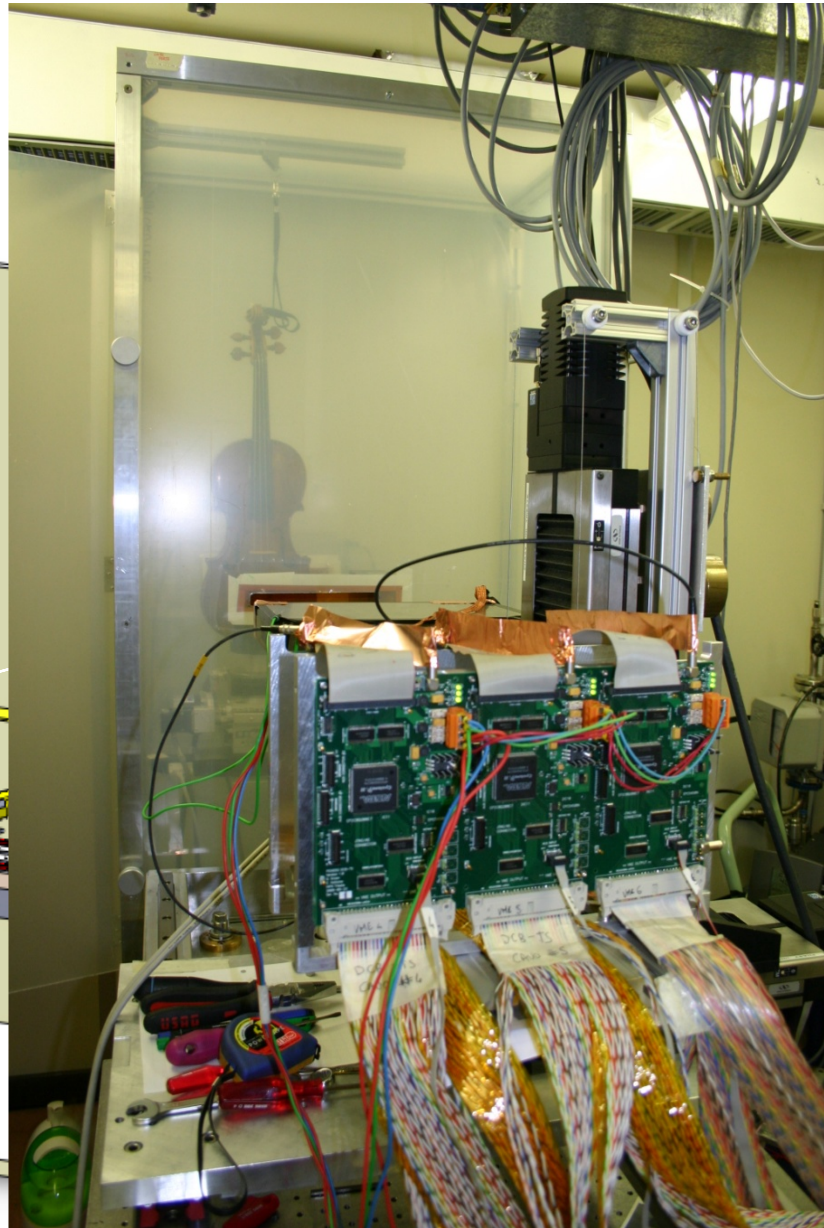

State-of-the-art clinical instrument of the Azienda Ospedaliera – University of Trieste

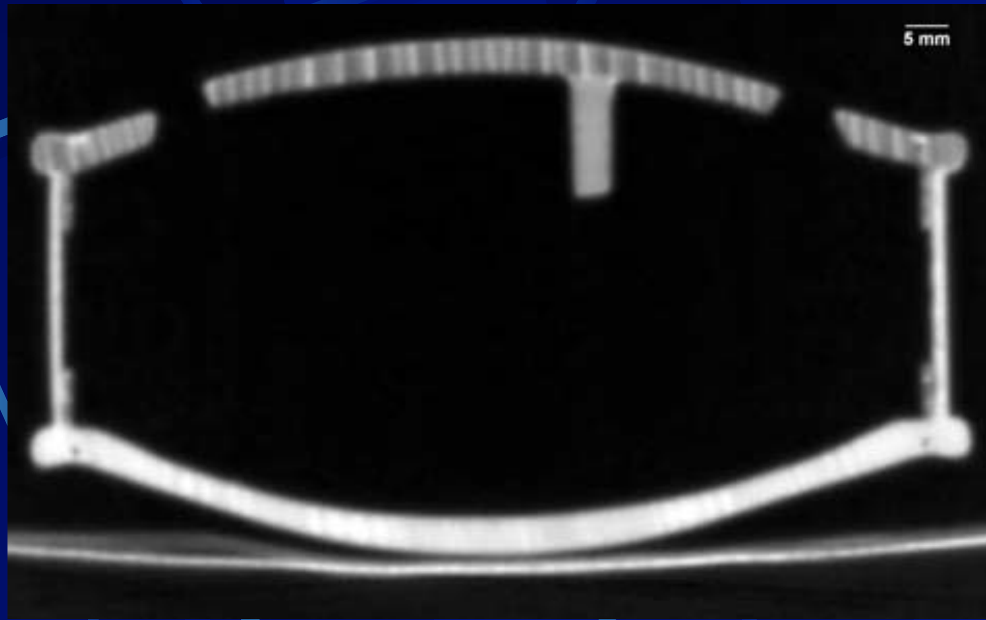

SYRMEP

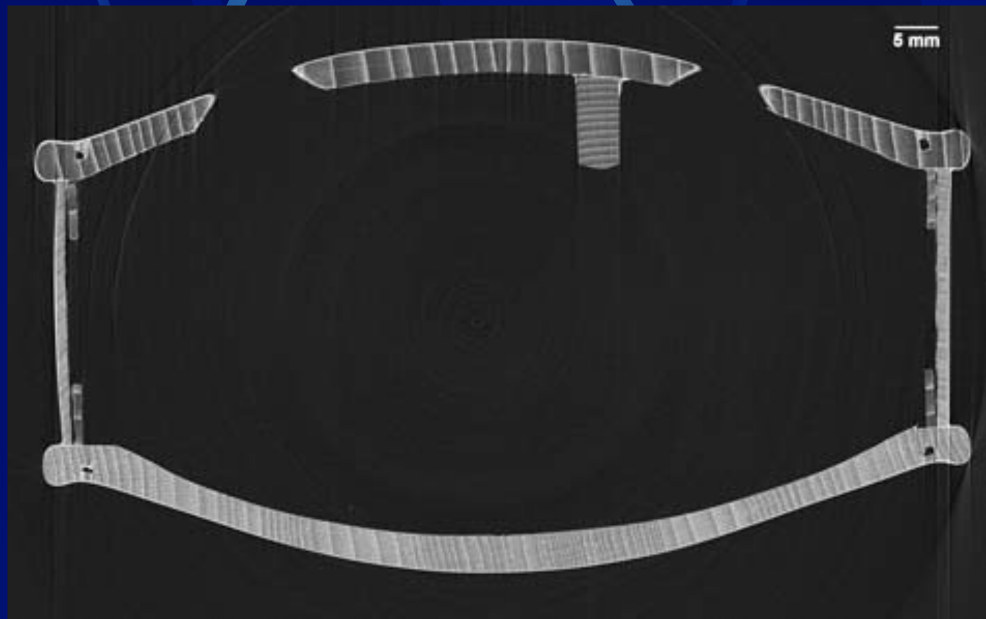

L. Rigon et al., e-Preservation Science, 7 (2010) 71-77.

Phytoremediation (from Ancient Greek *φυτο* (phyto), meaning "plant", and Latin *remedium*, meaning "restoring balance") describes the treatment of environmental problems (bioremediation) through the use of plants that mitigate the environmental problem without the need to excavate the contaminant material and dispose of it elsewhere.

Phytoremediation consists of mitigating pollutant concentrations in contaminated soils, water, or air, with plants able to contain, degrade, or eliminate metals, pesticides, solvents, explosives, crude oil and its derivatives, and various other contaminants from the media that contain them.

Phytoremediation

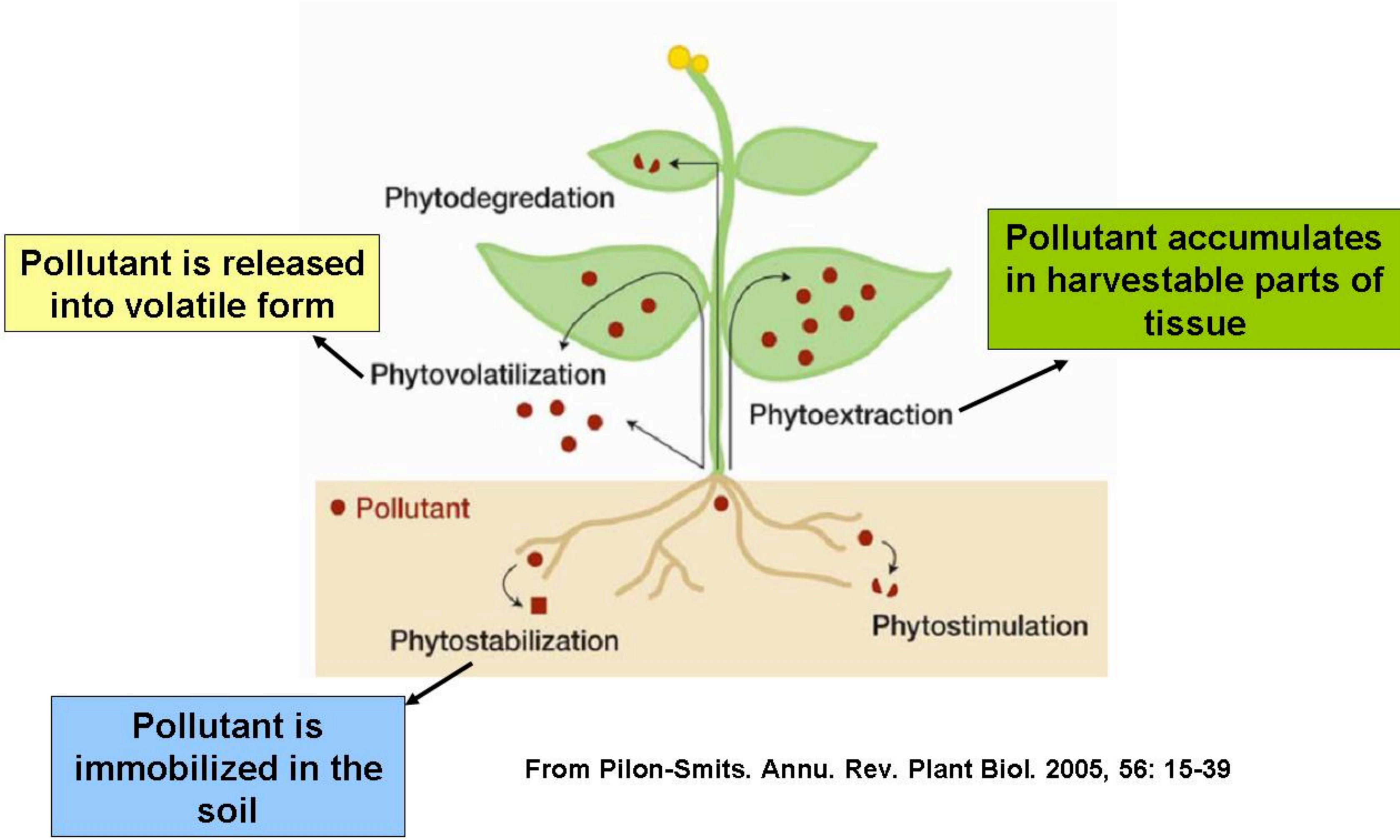

From Pilon-Smits. Annu. Rev. Plant Biol. 2005, 56: 15-39

Phytoremediation

The study of these problems presents various aspects, and consists in the detection of contaminants, in the comparison of accumulation properties of various plants and in the mapping of possible biological structures, which can specifically accumulate metals within a given tissue.

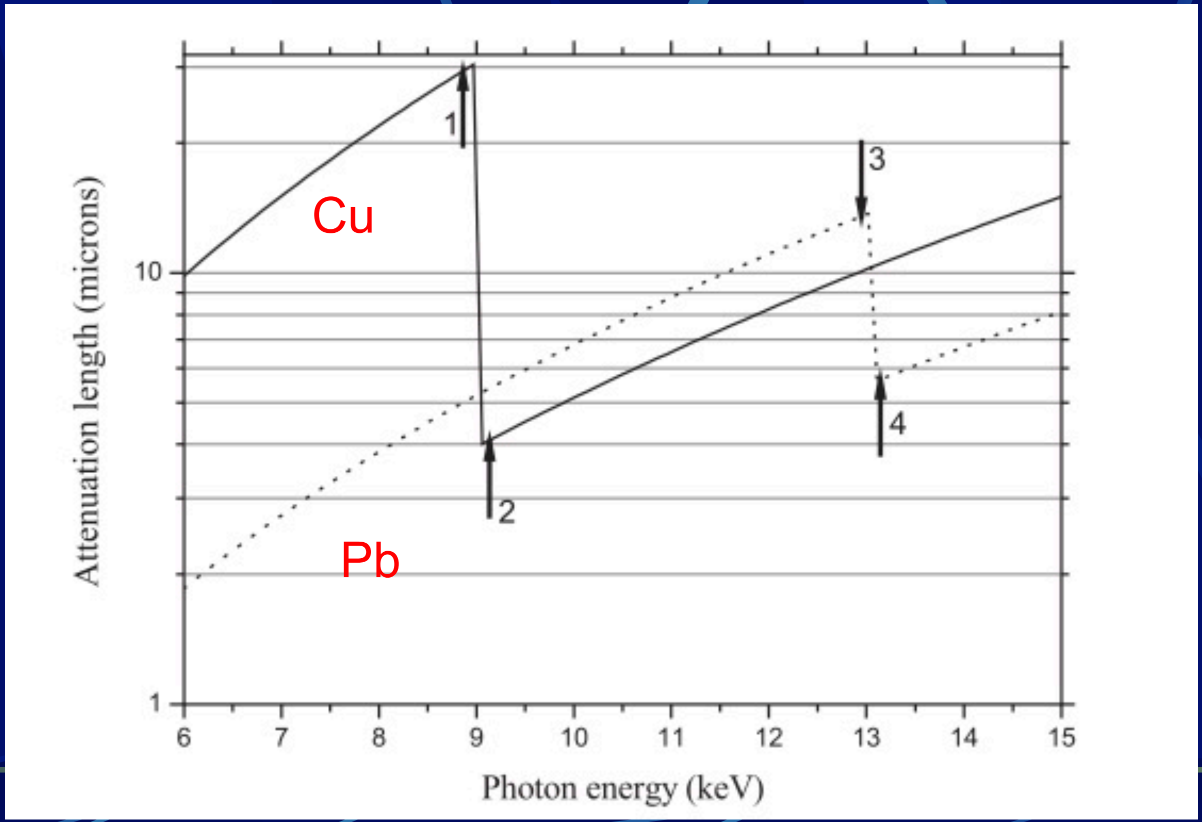

Phytoremediation and digital subtraction

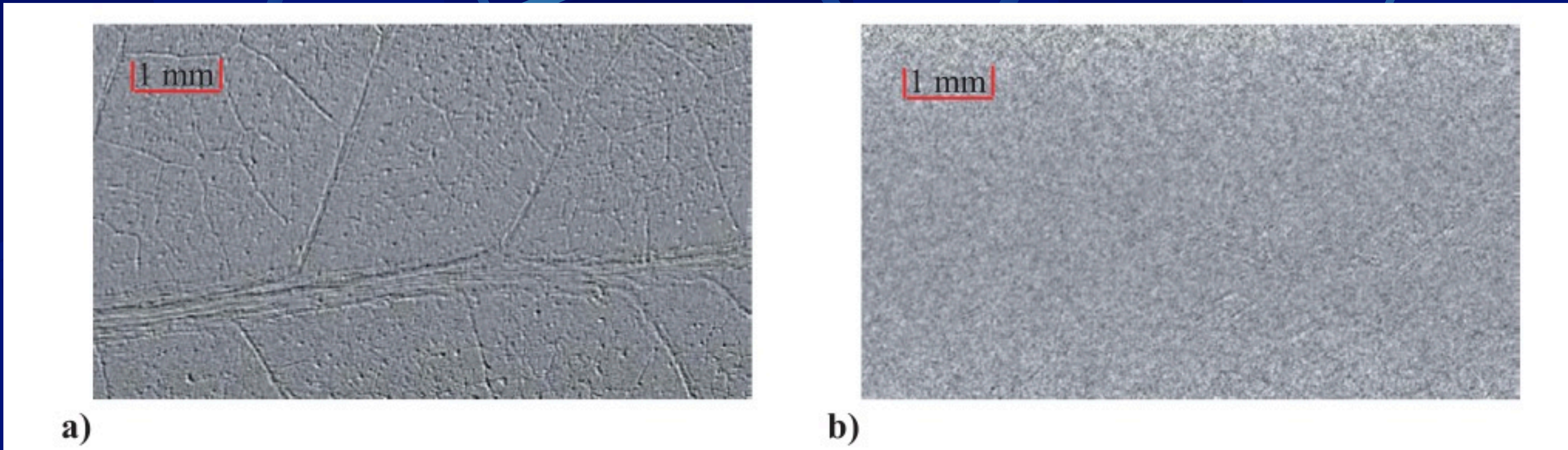

Pb detection by dual energy (13.150−12.975 keV), phase-contrast imaging at d = 168 cm in Helianthus annuus leaf, 15 days 10 mM PbAc treated (a), compared with untreated control sample (b).

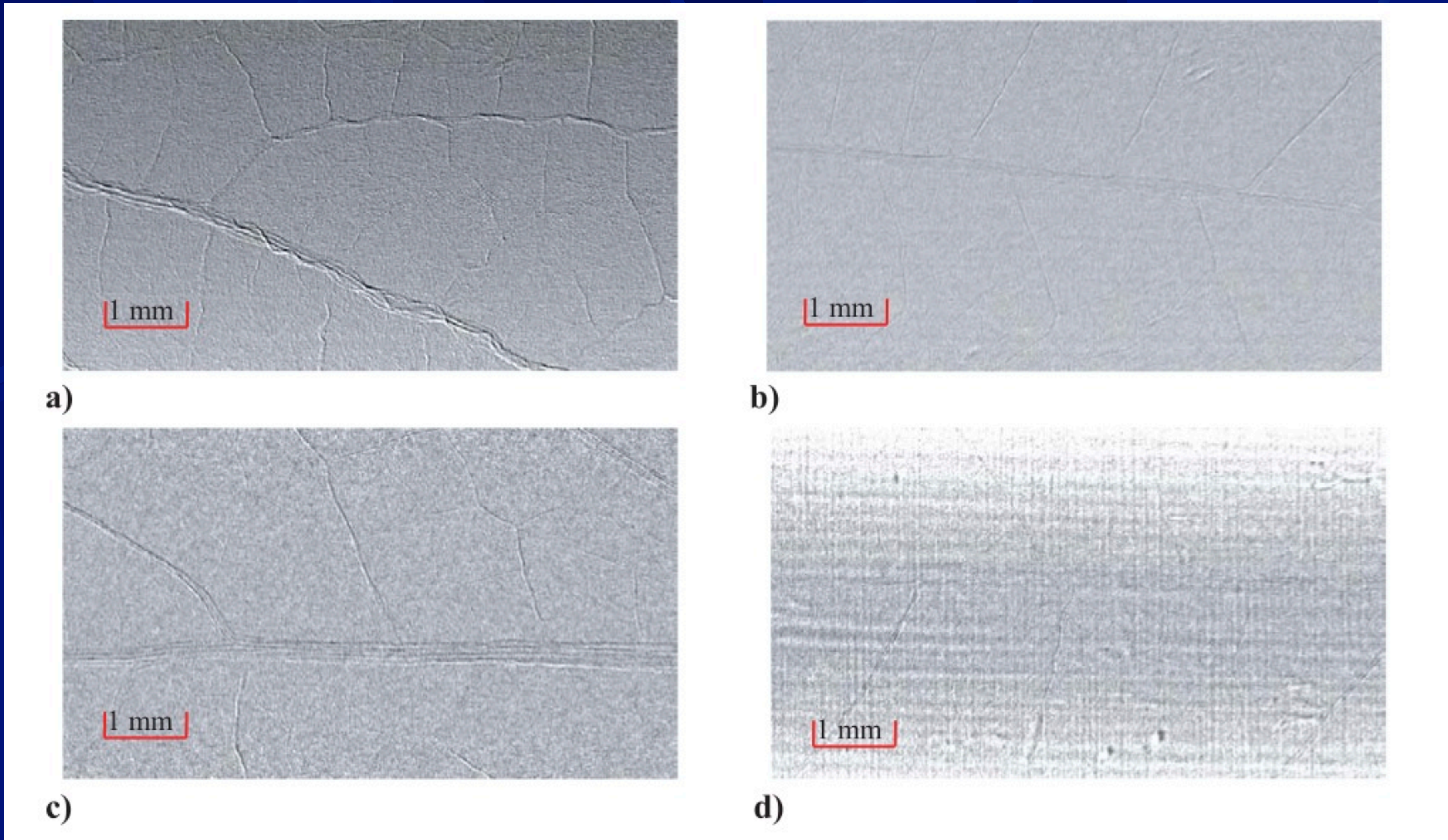

Cu detection by dual energy (9.05−8.90 keV) phase-contrast imaging at d = 35 cm in Phaseolus vulgaris leaf, 15 days 10 mM CuSO4 treated ethanol-fixed (a), compared with untreated ethanol-fixed control sample (b) together with 15 days 10 mM CuSO4 treated air dried sample (c), and untreated air-dried control sample (d).

Phytoremediation and digital subtraction

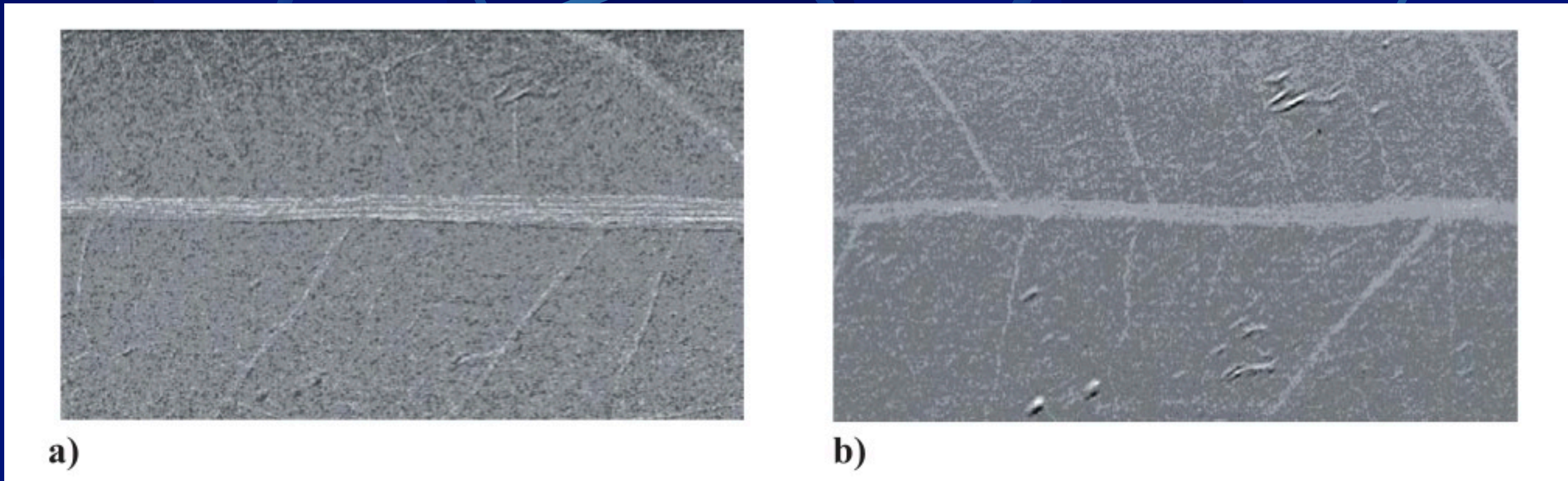

Cu detection by dual energy (9.05−8.90 keV) absorption imaging at d = 2 cm in Phaseolus Vulgaris leaf, 15 days 10 mM $CuSO_4$ treated ethanol-fixed (a), compared with air-dried sample (b).

a) b) c)

Preliminary results on the 3D reconstruction of a root of Dyplotaxis erucoides grown in 2% CuSO4 solution;

(a) differential planar radiograph

(b) and (c) reconstructions of the root fragments. The white arrows indicate the location of the Cu accumulation.

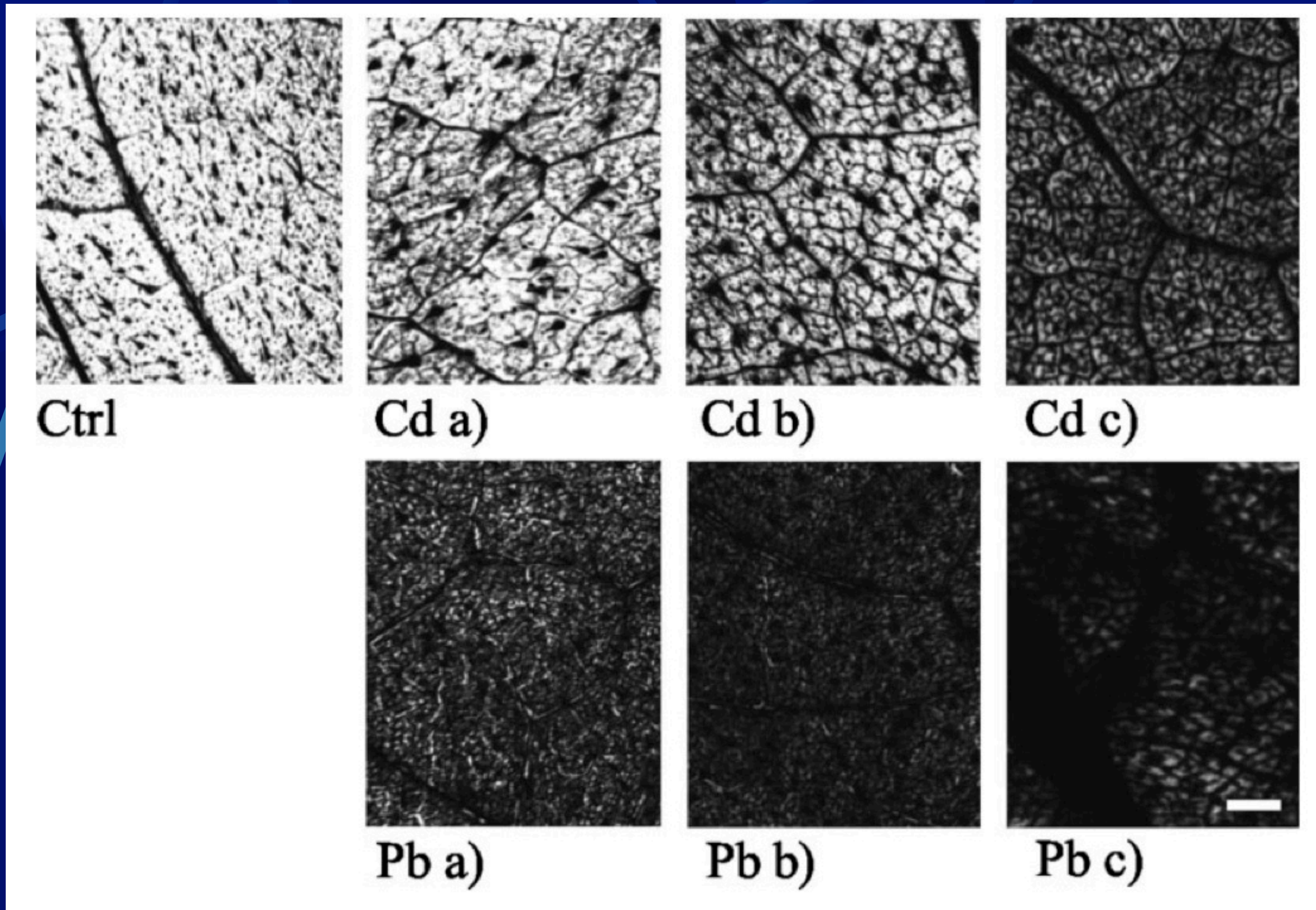

Radiographic images of the control (Ctrl) and of Helianthus annuus samples treated for 10 days with Cd or Pb salts of different concentrations: (a) 1, (b) 5, and (c) 10 mM. The length of the bar on the (c) image of Pb is 400 lm.

Phytoremediation and digital subtraction

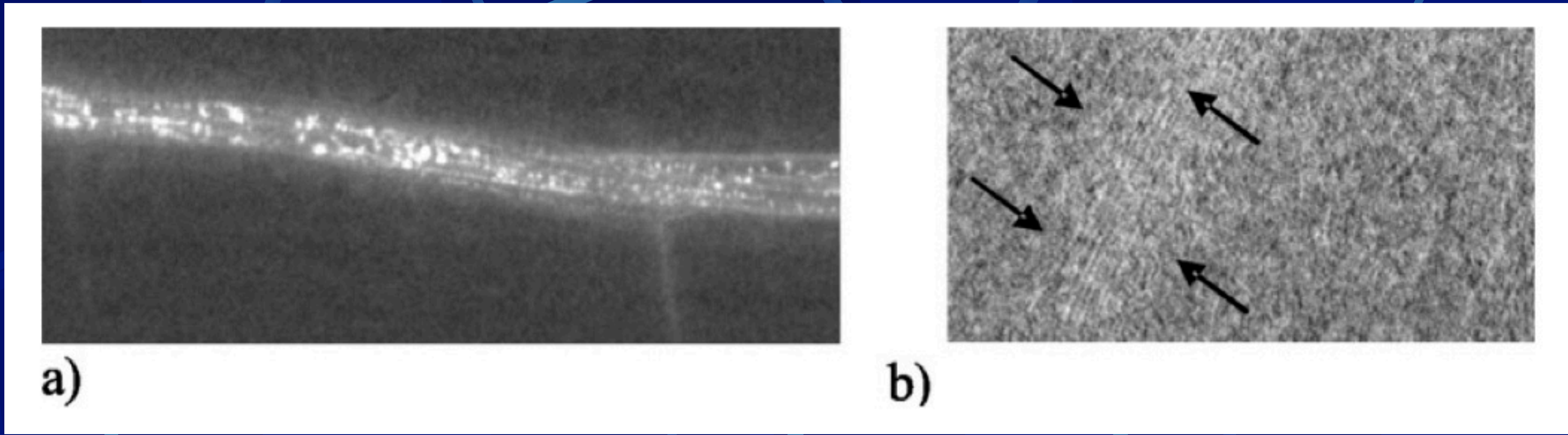

Result of the dual-energy analysis of metal detection in

(a) Pb-doped leaf sample

(b) Cd-doped leaf sample. The arrows indicate that the Cd is deposited in the leaf vein structure.

Phytoremediation and digital subtraction

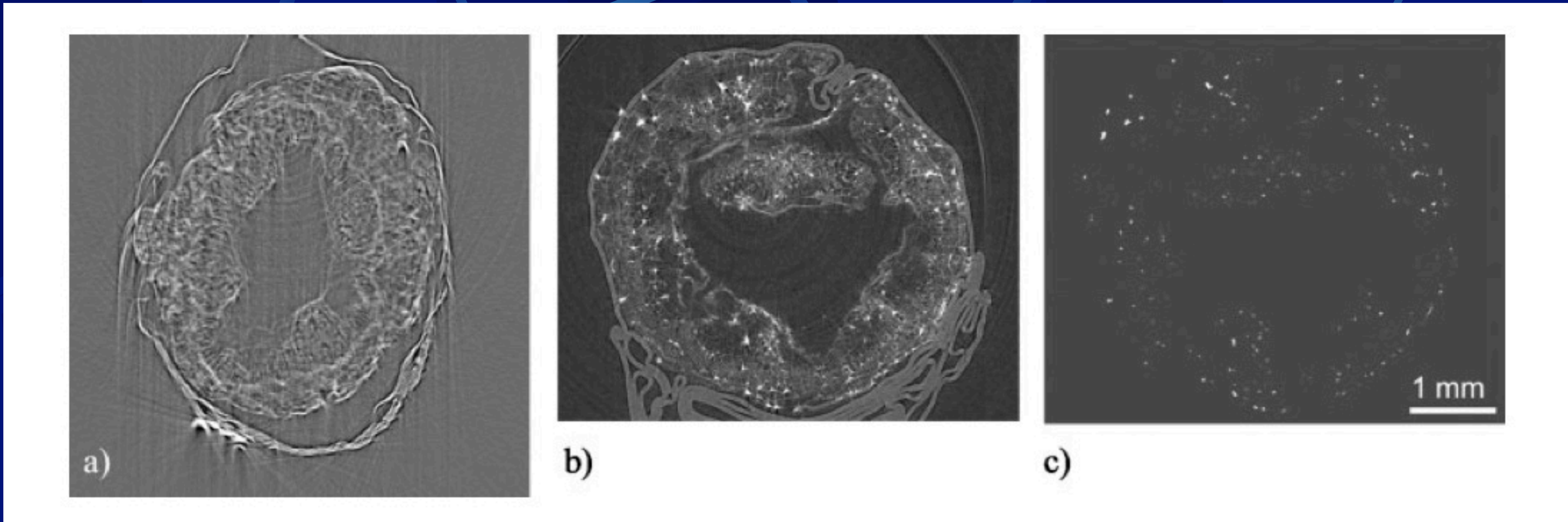

Slices of the Helianthus annuus root section.

(a) Control (untreated) sample exposed to radiation of energy 13.15 keV
(b) treated sample (1 day, 10 mM PbAc) exposed to radiation of energy 13.15 keV
(c) the map of the Pb deposition in this treated sample, obtained by dual energy difference measurements (13.15–12.975 keV). The samples were sectioned and picked up on Parafilm.

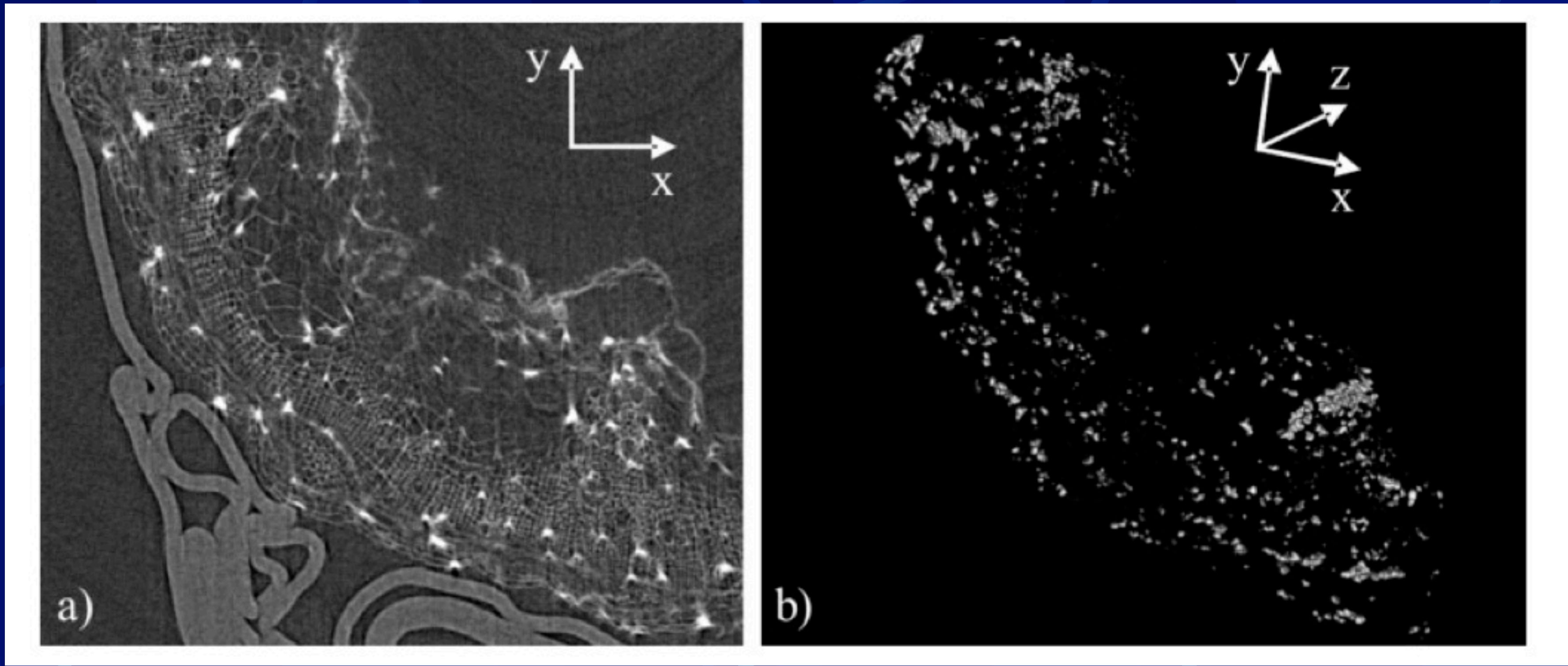

(a) Part of the root section showed in Figure 3b, together with the lead distribution in the appropriate volume of the sample.

(b) The thickness of the reconstructed volume was*1.5 mm(400 slices).